Measurement of the Turbulence Kinetic Energy Budget of a Turbulent Planar Wake Flow in Pressure Gradients

by

Xiaofeng Liu[†], Flint O. Thomas[‡] and Robert C. Nelson[‡]

Final Year-Three Report

Prepared for NASA Langley Research Center

Under Grant NAG 1-1878

[†] Graduate Research Assistant

[‡] Principal Investigator

Abstract

Turbulence kinetic energy (TKE) is a very important quantity for turbulence modeling and the budget of this quantity in its transport equation can provide insight into the flow physics. Turbulence kinetic energy budget measurements were conducted for a symmetric turbulent wake flow subjected to constant zero, favorable and adverse pressure gradients in year-three of research effort (NAG 1-1878). The purpose of this study is to clarify the flow physics issues underlying the demonstrated influence of pressure gradient on wake development and provide experimental support for turbulence modeling. To ensure the reliability of these notoriously difficult measurements, the experimental procedure was carefully designed on the basis of an uncertainty analysis. Four different approaches, based on an isotropic turbulence assumption, a locally axisymmetric homogeneous turbulence assumption (George and Hussein, 1991), a semi-isotropy assumption (Wygnanski and Fiedler, 1969) and a forced balance of the TKE equation, were applied for the estimate of the dissipation term. The pressure transport term is obtained from a forced balance of the turbulence kinetic energy equation. This report will present the results of the turbulence kinetic energy budget measurement and discuss their implication on the development of strained turbulent wakes.

Table of Contents

List of Figures

1. INTRODUCTION

1.1 Background and Review of the Notre Dame Wake Study

The three-year wake study project sponsored by NASA Langley Research Center and conducted at the University of Notre Dame is directly oriented to the high-lift application and is based on the "high-lift building block flow" concept[1-3]. The flow field over a multi-element airfoil is exceedingly complex and includes numerous viscous dominated effects. The basic idea of the high-lift building block flow concept is that the flow field over any multi-element airfoil may be broken down into certain generic component flows. These include 1) leading edge transition mechanism; 2) a variety of separated flow phenomena such as laminar separation bubbles and large-scale cove flow separation; 3) confluent boundary layer flow; 4) boundary layer and wake development in pressure gradients and with streamline curvature; 5) boundary layer relaminarization; and 6) multiple wake interactions. It is our position that the most useful approach to advance state-of-the-art in high-lift aerodynamics is to perform benchmark fluid dynamics experiments involving individual high-lift building block flows. Understanding high-lift building block flows individually is prerequisite to understanding their integrated behavior in a high-lift system.

Within the framework of the high-lift building block flow concept, the Notre Dame wake study is designed to simulate a particular kind of the high-lift building block flow, that is, the slat wake flow in a simplified yet more focused laboratory environment. More specifically, this wake research project is designed to investigate the symmetric/asymmetric planar wake flow development and structure subjected to a constant zero (ZPG), favorable (FPG) and adverse (APG) pressure gradient environment. The focus of this research project is based on the observation that there are two distinguishing features associated with the slat wake flow in a high-lift system. First, in a high-lift system, the slat wake development invariably occurs in a strong pressure gradient environment. Secondly, the slat wake profile is highly asymmetric in shape. It is expected that through a systematic experimental/numerical/analytical investigation into the symmetric/asymmetric wake development in pressure gradients, we can obtain a better understanding of the flow physics issues relevant to high-lift aerodynamics.

To date, the following work has been conducted at the University of Notre Dame for the wake research project:

- First year
  - Flow field survey of the symmetric wake in APG, ZPG and FPG.
- Second year
  - Flow field survey of the asymmetric wake in APG, ZPG and FPG.
  - Numerical simulation of symmetric and asymmetric wake in APG, ZPG and FPG.
- Third year
  - Similarity analysis of the symmetric wake mean flow in pressure gradient.
  - Intermittency investigation of the symmetric wake flow.

- Turbulence kinetic energy budget measurement of the symmetric wake in APG, ZPG and FPG.
- Uncertainty analysis of the TKE budget measurement and the LDV measurement.
- Space-time cross-correlation measurement of symmetric wake in APG, ZPG and FPG.

The first year research results were presented in a Year-One Report as well as in the AIAA paper 99-0677. The numerical simulations done during the second year may be found in Gregory Brooks' master thesis[4]. The rest of the results will appear in Xiaofeng Liu's Ph.D. thesis. This Year-Three Report will present the procedure, result, uncertainty analysis and discussion of the turbulence kinetic energy budget measurement of the symmetric wake in APG, ZPG and FPG. Measurement of the wake TKE budget was the primary focus of year-three activity.

1.2 Motivation and Objectives for the Turbulent Kinetic Energy Budget Measurement

By the conclusion of the second year of the wake study, a detailed database documenting the development of both initially symmetric and asymmetric wakes in zero, constant favorable and adverse pressure gradients had been completed. The extensive experimental database clearly shows the strong effect of pressure gradient and wake asymmetry on the near wake development[5,6]. Numerical simulations of this wake flow conducted at NASA Langley and at Notre Dame show that the existing turbulent models can capture the global wake development behavior such as wake widening and maximum velocity defect decay rate within a reasonable level of agreement[4,6,7]. However, the numerical simulation results also show that there is still room for the turbulence model to be improved.

As a natural consequence of the first two years of the investigation, detailed examination of the turbulent kinetic energy budget for the wake flow can greatly facilitate understanding of the observed effects of pressure and wake asymmetry on the wake flow development. In addition, the measurement of the turbulent kinetic energy budget for the wake flow in pressure gradient will be of interest in the development of more realistic turbulence models for turbulent flow. In brief, the TKE budget measurement of the wake study will fulfill the following research objectives:

- To understand the mechanism of the turbulence kinetic energy transport within the near wake flow;
- To investigate the influence of the pressure gradient on the turbulent kinetic energy transport and to provide an explanation for the observed effects of pressure gradient and wake asymmetry on the wake flow development;
- To provide experimental evidence for possible modification of turbulence model and/or the motivation for new approaches to numerically simulating the wake flow.

2. APPROACH FOR TURBULENT KINETIC ENERGY BUDGET MEASUREMENT

2.1 Transport Equation of the Turbulent Kinetic Energy

The TKE budget measurement scheme is motivated by previous attempts to characterize the turbulent kinetic energy budget in free shear flows, in particular, Wygnanski and Fiedler[8] (1969), Gutmark and Wygnanski[9] (1976), Panchapakesan and Lumley[10] (1993), Hussein, Capp and George[11] (1994) and Heskestad[12] (1965) in jet flows, Raffoul, Nejad and Gould[13] (1995) and Browne, Antonia and Shah[14] (1987) in bluff body wakes, Patel and Sarda[15] (1990) in a ship wake, Faure and Robert[16] (1969) in the wake of a self-propelled body, Wygnanski and Fiedler[17] (1970) in a planar mixing layer, Zhou, Heine and Wygnanski[18] (1996) in a plane wall jet and George and Hussein[19] (1991) in a round jet. Before introducing the TKE budget measurement scheme, it is necessary to first discuss the TKE transport equations in the following paragraphs.

From Hinze[20] (1975, p.72, Equation 1-110), the turbulent kinetic energy equation can be written as

$$\underset{\text{I}}{\frac{D}{Dt}\left(\frac{\overline{q^2}}{2}\right)} = \underset{\text{II}}{-\frac{\partial}{\partial x_i}\overline{u_i'\left(\frac{p'}{\rho}+\frac{q^2}{2}\right)}} \underset{\text{III}}{-\overline{u_i'u_j'}\frac{\partial \overline{U_j}}{\partial x_i}} \underset{\text{IV}}{+\nu\frac{\partial}{\partial x_i}\overline{u_j'\left(\frac{\partial u_i'}{\partial x_j}+\frac{\partial u_j'}{\partial x_i}\right)}} \underset{\text{V}}{-\nu\overline{\left(\frac{\partial u_i'}{\partial x_j}+\frac{\partial u_j'}{\partial x_i}\right)\frac{\partial u_j'}{\partial x_i}}} \quad (1)$$

where u_i' is the turbulent fluctuating velocity component, p' is the fluctuating pressure, and $\frac{1}{2}\overline{q^2} \equiv \frac{1}{2}\overline{u_i'u_i'} = k$ is the turbulent kinetic energy per unit mass. Term I on the left hand side of equation (1) represents the convection of turbulent kinetic energy along mean flow stream lines. Term II represents the transport of turbulent kinetic energy by both the turbulent velocity fluctuations themselves and by pressure fluctuations. Term III represents turbulent kinetic energy production by the Reynolds stress working aganst the mean strain rate. Term IV represents viscous diffusion of turbulence. Term V represents the viscous dissipation of turbulent kinetic energy into heat.

For incompressible, homogeneous turbulent flow, the turbulent kinetic energy equation takes the form (Hinze[20] 1975, p.74, Equation 1-111),

$$\underset{\text{I}}{\frac{D}{Dt}\left(\frac{\overline{q^2}}{2}\right)} = \underset{\text{II}}{-\frac{\partial}{\partial x_i}\overline{u_i'\left(\frac{p'}{\rho}+\frac{q^2}{2}\right)}} \underset{\text{III}}{-\overline{u_i'u_j'}\frac{\partial \overline{U_j}}{\partial x_i}} \underset{\text{IV}}{+\frac{\nu}{2}\frac{\partial^2 \overline{q^2}}{\partial x_i \partial x_i}} \underset{\text{V}}{-\nu\overline{\frac{\partial u_j'}{\partial x_i}\frac{\partial u_j'}{\partial x_i}}} \quad (2)$$

where Terms I, II and III are the same as those in Equation (1), whereas Terms IV and V take different forms of their counterparts in Equation (1). For free shear flows, Term IV, the visocous diffusion term, is usually negligible compared to other terms. Therefore, the only accountable difference between Equations (1) and (2) for free shear flows is the last term, i.e., the dissipation term.

We will denote the streamwise, lateral and spanwise spatial coordinates as x_1, x_2 and x_3, respectively. Later on, the spatial coordinates x_1, x_2 and x_3, the velocity components U_1, U_2 and U_3 and the fluctuating velocity components u_1', u_2' and u_3' will be represented by x, y, z, U, V, W, u, v and w respectively for convenience.

Expansion of the dissipation term in equation (1) gives

$$\varepsilon_{non-homo} = \nu\left\{2\overline{\left(\frac{\partial u_1'}{\partial x_1}\right)^2} + \overline{\left(\frac{\partial u_2'}{\partial x_1}\right)^2} + \overline{\left(\frac{\partial u_3'}{\partial x_1}\right)^2} + \overline{\left(\frac{\partial u_1'}{\partial x_2}\right)^2} + 2\overline{\left(\frac{\partial u_2'}{\partial x_2}\right)^2} + \overline{\left(\frac{\partial u_3'}{\partial x_2}\right)^2} + \overline{\left(\frac{\partial u_1'}{\partial x_3}\right)^2} + \overline{\left(\frac{\partial u_2'}{\partial x_3}\right)^2} + 2\overline{\left(\frac{\partial u_3'}{\partial x_3}\right)^2}\right.$$
$$\left. + 2\overline{\left(\frac{\partial u_1'}{\partial x_2}\right)\left(\frac{\partial u_2'}{\partial x_1}\right)} + 2\overline{\left(\frac{\partial u_1'}{\partial x_3}\right)\left(\frac{\partial u_3'}{\partial x_1}\right)} + 2\overline{\left(\frac{\partial u_2'}{\partial x_3}\right)\left(\frac{\partial u_3'}{\partial x_2}\right)}\right\} \quad (3)$$

Similarly, expansion of the dissipation term in equation (2) gives

$$\varepsilon_{homo} = \nu\left(\overline{\left(\frac{\partial u_1'}{\partial x_1}\right)^2} + \overline{\left(\frac{\partial u_2'}{\partial x_1}\right)^2} + \overline{\left(\frac{\partial u_3'}{\partial x_1}\right)^2} + \overline{\left(\frac{\partial u_1'}{\partial x_2}\right)^2} + \overline{\left(\frac{\partial u_2'}{\partial x_2}\right)^2} + \overline{\left(\frac{\partial u_3'}{\partial x_2}\right)^2} + \overline{\left(\frac{\partial u_1'}{\partial x_3}\right)^2} + \overline{\left(\frac{\partial u_2'}{\partial x_3}\right)^2} + \overline{\left(\frac{\partial u_3'}{\partial x_3}\right)^2}\right) \quad (4)$$

To date, no one has been able to successfully measure the cross derivative correlation terms in the non-homogeneous form of the dissipation as listed in Equation (3), though there was an attempt by Browne, Antonia and Shah[14] (1987). Fortunately, in many circumstances, the cross derivative correlation terms are not so crucial compared to other terms in the determination of the dissipation and the homogeneous dissipation expression is good enough to lead to a satisfactory result. In other words, the determination of the cross derivative correlation terms can be encompassed by the homogeneous consideration. As all previous reported efforts for the direct measurement of the dissipation term, in our research project, we will only consider Equation (2). With the aforementioned notations, Equation (2) can be expanded as,

$$\frac{\partial}{\partial t}\left(\frac{\overline{q^2}}{2}\right)+\overline{U_1}\frac{\partial}{\partial x_1}\left(\frac{\overline{q^2}}{2}\right)+\overline{U_2}\frac{\partial}{\partial x_2}\left(\frac{\overline{q^2}}{2}\right)+\overline{U_3}\frac{\partial}{\partial x_3}\left(\frac{\overline{q^2}}{2}\right)=$$
$$-\frac{\partial}{\partial x_1}\overline{u_1'\frac{p'}{\rho}}-\frac{\partial}{\partial x_2}\overline{u_2'\frac{p'}{\rho}}-\frac{\partial}{\partial x_3}\overline{u_3'\frac{p'}{\rho}}-\frac{\partial}{\partial x_1}\overline{\frac{1}{2}\left(u_1'^3+u_1'u_2'^2+u_1'u_3'^2\right)}$$
$$-\frac{\partial}{\partial x_2}\overline{\frac{1}{2}\left(u_1'^2u_2'+u_2'^3+u_2'u_3'^2\right)}-\frac{\partial}{\partial x_3}\overline{\frac{1}{2}\left(u_1'^2u_3'+u_2'^2u_3'+u_3'^3\right)}$$
$$-\overline{u_1'^2}\frac{\partial\overline{U_1}}{\partial x_1}-\overline{u_1'u_2'}\frac{\partial\overline{U_2}}{\partial x_1}-\overline{u_1'u_3'}\frac{\partial\overline{U_3}}{\partial x_1}-\overline{u_1'u_2'}\frac{\partial\overline{U_1}}{\partial x_2}-\overline{u_2'^2}\frac{\partial\overline{U_2}}{\partial x_2}-\overline{u_2'u_3'}\frac{\partial\overline{U_3}}{\partial x_2}$$
$$-\overline{u_1'u_3'}\frac{\partial\overline{U_1}}{\partial x_3}-\overline{u_2'u_3'}\frac{\partial\overline{U_2}}{\partial x_3}-\overline{u_3'^2}\frac{\partial\overline{U_3}}{\partial x_3}$$
$$+\frac{\nu}{2}\frac{\partial^2\overline{q^2}}{\partial x_1^2}+\frac{\nu}{2}\frac{\partial^2\overline{q^2}}{\partial x_2^2}+\frac{\nu}{2}\frac{\partial^2\overline{q^2}}{\partial x_3^2}$$
$$-\nu\overline{\left(\left(\frac{\partial u_1'}{\partial x_1}\right)^2+\left(\frac{\partial u_1'}{\partial x_2}\right)^2+\left(\frac{\partial u_1'}{\partial x_3}\right)^2+\left(\frac{\partial u_2'}{\partial x_1}\right)^2+\left(\frac{\partial u_2'}{\partial x_2}\right)^2+\left(\frac{\partial u_2'}{\partial x_3}\right)^2+\left(\frac{\partial u_3'}{\partial x_1}\right)^2+\left(\frac{\partial u_3'}{\partial x_2}\right)^2+\left(\frac{\partial u_3'}{\partial x_3}\right)^2\right)} \quad (5)$$

For steady, 2-D flow in the mean, we have $\frac{\partial}{\partial t}(\overline{\ })=0$, $\overline{U_3}=0$ and $\frac{\partial}{\partial x_3}(\overline{\ })=0$. Also we have, from the continuity equation, $\frac{\partial\overline{U_2}}{\partial x_2}=-\frac{\partial\overline{U_1}}{\partial x_1}$. Thus, the turbulent kinetic energy equation can be simplified as follows:

$$\underbrace{\overline{U_1}\frac{\partial}{\partial x_1}\left(\frac{\overline{q^2}}{2}\right)+\overline{U_2}\frac{\partial}{\partial x_2}\left(\frac{\overline{q^2}}{2}\right)=}_{\text{Convection}}$$
$$\underbrace{-\frac{\partial}{\partial x_1}\overline{u_1'\frac{p'}{\rho}}-\frac{\partial}{\partial x_2}\overline{u_2'\frac{p'}{\rho}}}_{\text{Pressure Diffusion}}\quad\underbrace{-\frac{\partial}{\partial x_1}\overline{\frac{1}{2}\left(u_1'^3+u_1'u_2'^2+u_1'u_3'^2\right)}-\frac{\partial}{\partial x_2}\overline{\frac{1}{2}\left(u_1'^2u_2'+u_2'^3+u_2'u_3'^2\right)}}_{\text{Turbulence Diffusion}}$$
$$\underbrace{-\left(\overline{u_1'^2}-\overline{u_2'^2}\right)\frac{\partial\overline{U_1}}{\partial x_1}-\overline{u_1'u_2'}\left(\frac{\partial\overline{U_1}}{\partial x_2}+\frac{\partial\overline{U_2}}{\partial x_1}\right)}_{\text{Production}}\quad\underbrace{+\frac{\nu}{2}\frac{\partial^2\overline{q^2}}{\partial x_1^2}+\frac{\nu}{2}\frac{\partial^2\overline{q^2}}{\partial x_2^2}}_{\text{Viscous Diffusion}}$$
$$\underbrace{-\nu\overline{\left(\left(\frac{\partial u_1'}{\partial x_1}\right)^2+\left(\frac{\partial u_1'}{\partial x_2}\right)^2+\left(\frac{\partial u_1'}{\partial x_3}\right)^2+\left(\frac{\partial u_2'}{\partial x_1}\right)^2+\left(\frac{\partial u_2'}{\partial x_2}\right)^2+\left(\frac{\partial u_2'}{\partial x_3}\right)^2+\left(\frac{\partial u_3'}{\partial x_1}\right)^2+\left(\frac{\partial u_3'}{\partial x_2}\right)^2+\left(\frac{\partial u_3'}{\partial x_3}\right)^2\right)}}_{\text{Dissipation}} \quad (6)$$

A primary effort for year-three is to successfully measure the individual terms in the above 2-D simplified incompressible homogeneous TKE transport equation.

2.2 Approaches for the Measurement of the Turbulent Kinetic Energy Budget

The procedure used for the experimental estimate of each term in turbulent kinetic energy balance will be outlined below.

2.2.1 Convection Terms

According to the literature, the convection terms are usually obtained from direct measurement. In this wake study, this term will be obtained by use of X-wire probe. In particular, the streamwise spatial derivative $\frac{\partial}{\partial x_1}\left(\frac{\overline{q^2}}{2}\right)$ will be evaluated from the measurement of $\overline{q^2}$ at three adjacent streamwise measurement stations. The lateral spatial derivative $\frac{\partial}{\partial x_2}\left(\frac{\overline{q^2}}{2}\right)$ will be obtained from lateral survey data.

2.2.2 Pressure Diffusion Terms

This term is not directly measurable. In the jet studies by Wygnanski and Fiedler (1969) and Gutmark and Wygnanski (1976), this term was inferred from the balance of the turbulent kinetic energy equation. In the more recent axisymmetric jet study by Panchapakesan and Lumley (1993), the pressure transport term was simply neglected. In a cylinder wake study by Browne, Antonia and Shah (1987), they demonstrated that the pressure transport term obtained by forcing a balance of the turbulent kinetic energy equation approximates to zero. In the measurement for a jet flow conducted by Hussein, Capp and George(1994), they ignored the term $\overline{\left(\frac{u_1' p'}{\rho}\right)}$ and attempted to estimate $\overline{\left(\frac{u_2' p'}{\rho}\right)}$ by integrating the difference of the so-called "transport dissipation" and the "homogeneous dissipation". In this study, this term will be inferred from the forced balance of the turbulent kinetic energy equation.

2.2.3 Turbulence Diffusion Terms

An X-wire probe can be used to obtain $\overline{u_1'^3}$, $\overline{u_1' u_2'^2}$, $\overline{u_1' u_3'^2}$, $\overline{u_1'^2 u_2'}$ and $\overline{u_1'^3}$ by direct measurement. The remaining term $\overline{u_2' u_3'^2}$ can be obtained indirecly from additional X-wire measurements through application of a procedure developed by Townsend (1949) and described by Wygnanski and Fiedler (1969). Alternately, both Panchapakesan and Lumley (1993) and Hussein, Capp and George (1994) simply assumed that $\overline{u_2' u_3'^2} \approx \overline{u_3'^3}$ for their jet flow measurements, and asserted that the error introduced by this assumption is less than 10%. In this study, we will also use the X-wire measuerement to obtain the turbulence diffusion term with the assumption that $\overline{u_2' u_3'^2} \approx \overline{u_3'^3}$.

2.2.4 Production Terms

The shear and dilatational production terms have already been measured in year-one and year-two of the wake study for both symmetric and asymmetric wakes using an Aerometrics LDV system in two-component coincidence mode. These experiments show

that, despite the streamwise pressure gradients imposed, the wake is shear dominated. That is, $-\left(\overline{u_1'^2}-\overline{u_2'^2}\right)\frac{\partial \overline{U_1}}{\partial x_1} << -\overline{u_1'u_2'}\left(\frac{\partial \overline{U_1}}{\partial x_2}+\frac{\partial \overline{U_2}}{\partial x_1}\right)$ in each case. For this study, these terms will be measured again by using the X-wire probe in order to ensure repeatability.

2.2.5 Viscous Diffusion Terms

All previously cited investigations of turbulent kinetic energy budget in free shear flows have ignored the viscous diffusion terms. Wygnanski and Fiedler (1969) and Gutmark and Wygnanski (1976) claim the neglect of these terms was based on the assertion of Laufer(1954) that these types of terms are comparatively small in the turbulent kinetic energy equation. Panchapakesan and Lumley (1993) explained that in free turbulent flows, away from walls, the viscous contribution to the transport terms are negligible in comparison with the turbulent contribution. In high Reynolds number free shear flows, like the wake studied here, the viscous diffusion is expected to be negligible.

2.2.6 Dissipation Terms

The viscous dissipation terms could be handled in one of the following five ways, according to the lterature.

1) *Isotropic Turbulence Assumption*: If it is assumed that viscous dissipation takes place at the smallest scales of motion which may be approximated as locally isotropic, then the visocus dissipation term simplifies to,

$$\varepsilon = 15\nu\overline{\left(\frac{\partial u_1'}{\partial x_1}\right)^2} \tag{7}$$

The fluctuating spatial derivative can be obtained by invoking the Taylor's frozen field hypothesis

$$\frac{\partial}{\partial x} \approx -\frac{1}{\overline{U_1}}\frac{\partial}{\partial t} \tag{8}$$

This was the technique employed by Gutmark and Wygnanski (1976) for their jet flow measurement.

2) *Locally Axisymmetric Homogeneous Turbulence Assumption*: This is an approach proposed by George and Hussein (1991). They demonstrated that as long as the time averaged derivatives in the dissipation term (3) satisfy the following conditions for the so-called locally axisymmetric homogeneous turbulence,

$$\overline{\left(\frac{\partial u_1'}{\partial x_2}\right)^2} = \overline{\left(\frac{\partial u_1'}{\partial x_3}\right)^2} \tag{9}$$

$$\overline{\left(\frac{\partial u_2'}{\partial x_1}\right)^2} = \overline{\left(\frac{\partial u_3'}{\partial x_1}\right)^2} \tag{10}$$

$$\overline{\left(\frac{\partial u_2'}{\partial x_2}\right)^2} = \overline{\left(\frac{\partial u_3'}{\partial x_3}\right)^2} \tag{11}$$

$$\overline{\left(\frac{\partial u_2'}{\partial x_3}\right)^2} = \overline{\left(\frac{\partial u_3'}{\partial x_2}\right)^2} \tag{12}$$

$$\overline{\left(\frac{\partial u_2'}{\partial x_2}\right)^2} = \frac{1}{3}\overline{\left(\frac{\partial u_1'}{\partial x_1}\right)^2} + \frac{1}{3}\overline{\left(\frac{\partial u_2'}{\partial x_3}\right)^2} \tag{13}$$

$$\overline{\left(\frac{\partial u_2'}{\partial x_3}\right)\left(\frac{\partial u_3'}{\partial x_2}\right)} = \frac{1}{6}\overline{\left(\frac{\partial u_1'}{\partial x_1}\right)^2} - \frac{1}{3}\overline{\left(\frac{\partial u_2'}{\partial x_3}\right)^2} \tag{14}$$

$$\overline{\left(\frac{\partial u_1'}{\partial x_2}\right)\left(\frac{\partial u_2'}{\partial x_1}\right)} = \overline{\left(\frac{\partial u_1'}{\partial x_3}\right)\left(\frac{\partial u_3'}{\partial x_1}\right)} = -\frac{1}{2}\overline{\left(\frac{\partial u_1'}{\partial x_1}\right)^2} \tag{15}$$

then the dissipation term can be estimated from either

$$\varepsilon = \nu\left(\frac{5}{3}\overline{\left(\frac{\partial u_1'}{\partial x_1}\right)^2} + 2\overline{\left(\frac{\partial u_1'}{\partial x_3}\right)^2} + 2\overline{\left(\frac{\partial u_2'}{\partial x_1}\right)^2} + \frac{8}{3}\overline{\left(\frac{\partial u_2'}{\partial x_3}\right)^2}\right) \tag{16}$$

or

$$\varepsilon = \nu\left(-\overline{\left(\frac{\partial u_1'}{\partial x_1}\right)^2} + 2\overline{\left(\frac{\partial u_1'}{\partial x_2}\right)^2} + 2\overline{\left(\frac{\partial u_2'}{\partial x_1}\right)^2} + 8\overline{\left(\frac{\partial u_2'}{\partial x_2}\right)^2}\right) \tag{17}$$

In Equation (16), the $\overline{\left(\frac{\partial u_1'}{\partial x_1}\right)^2}$ and the $\overline{\left(\frac{\partial u_1'}{\partial x_3}\right)^2}$ terms can be obtained from the parallel probe measurement while the $\overline{\left(\frac{\partial u_2'}{\partial x_1}\right)^2}$ term can be obtained from an X-wire measurement. The estimate of the $\overline{\left(\frac{\partial u_2'}{\partial x_3}\right)^2}$ term requires a twin X-wire probe configuration, which will be dissused in details in Section 3.4 and 4.2.4.2.

3) *Semi-Isotropic Turbulence Assumption*: This is an approach for the the estimate of unmeasured or unmeasurable fluctuating velocity derivatives in the homogeneous dissipation term based on measured fluctuating velocity derivatives. For example, the streamwise derivatives $\overline{\left(\frac{\partial u_1'}{\partial x_1}\right)^2}$, $\overline{\left(\frac{\partial u_2'}{\partial x_1}\right)^2}$ and $\overline{\left(\frac{\partial u_3'}{\partial x_1}\right)^2}$ can be each estimated by invoking the Taylor's hypothesis as descibed above. The lateral and spanwise derivatives, $\overline{\left(\frac{\partial u_1'}{\partial x_2}\right)^2}$ and $\overline{\left(\frac{\partial u_1'}{\partial x_3}\right)^2}$ can be obtained by a closely spaced parallel hot-wire probes. The four remaining derivatives $\overline{\left(\frac{\partial u_2'}{\partial x_2}\right)^2}$, $\overline{\left(\frac{\partial u_2'}{\partial x_3}\right)^2}$, $\overline{\left(\frac{\partial u_3'}{\partial x_2}\right)^2}$ and $\overline{\left(\frac{\partial u_3'}{\partial x_3}\right)^2}$ in the dissipation term can be subsequently estimated by invoking a semi-isotropy assumption, as described in Wygnanski and Fiedler (1969) for their jet flow measurement, which assumes the nine spatial derivatives in the dissipation term observe the following semi-isotropy relationship:

$$
\begin{aligned}
k_s\overline{\left(\frac{\partial u_1'}{\partial x_1}\right)^2} &= \overline{\left(\frac{\partial u_2'}{\partial x_1}\right)^2} = \overline{\left(\frac{\partial u_3'}{\partial x_1}\right)^2} \\
\overline{\left(\frac{\partial u_1'}{\partial x_2}\right)^2} &= k_s\overline{\left(\frac{\partial u_2'}{\partial x_2}\right)^2} = \overline{\left(\frac{\partial u_3'}{\partial x_2}\right)^2} \\
\overline{\left(\frac{\partial u_1'}{\partial x_3}\right)^2} &= \overline{\left(\frac{\partial u_2'}{\partial x_3}\right)^2} = k_s\overline{\left(\frac{\partial u_3'}{\partial x_3}\right)^2}
\end{aligned}
\tag{18}
$$

where k_s is the semi-isotropy coefficient. In the jet investigation conducted by Wygnanski and Fiedler(1969), they took $k_s = 1 + e^{-200y^2}$, with the assumption that the isotropic relations hold for the mean square derivatives with respect to a given direction in the jet center and there is a tendency towards anisotropy in the off-center region. In this study, the coefficient k_s will be determined from the streamwise mean square derivative measuremets, which will be described in details in Section 4.

4) *Direct Measurement of All Nine Terms*: The most sophisticated method is to measure all nine terms that make up the total dissipation by use of two X-wires as descibed by Browne, Antonia and Shah (1987) for their cylinder wake study. Their study indicated that the local isotropy assumption is not valid for a cylinder wake in the self-preserving region with relatively low Reynolds number. Keep in mind that it is the local isotropy assumption that forms the basis of the first method mentioned above for evaluating the dissipation terms. It should be very interesting to verify the local isotropy assumption for the wake development in pressure gradients at high Reynolds number. In this study, we feel that the spatial resolution of the 2 X-wire probe configuration is too large to get a reliable dissipation measurement, therefore we will not use this approach to measure the dissipation term.

5) *Forced Balance of the TKE Equation*: Finally, the easiest way to evaluate the dissipation terms might be forcing a balance of the turbulent kinetic energy equation, provided that the pressure transport terms are negligible. This was the approach taken by Panchapakesan and Lumley(1993).

In the wake study here, the dissipation term will be estimated by using all of the above except the fourth approaches. The results will then be compared and reviewed in the context of the TKE balance.

3. EXPERIMENTAL SETUP AND MEASUREMENT SCHEME

3.1 Wind Tunnel and Model Geometry

3.1.1 Wind Tunnel

The experiments were performed in an in-draft subsonic wind tunnel facility located at the Hessert Center for Aerospace Research at the University of Notre Dame. The

schematic of the wind tunnel is shown in Figure 1. Ambient laboratory air is drawn into a contraction inlet with 9 ft. by 9 ft. effective area by an eight-bladed fan connected to an 18.6kW AC induction motor. The contraction ratio of the tunnel inlet is 20.25:1 with 12 anti-turbulence screens, which leads to a uniform test section inlet velocity profile with low turbulence intensity level(less than 0.1% with signal high-pass filtered at 3Hz and less than 0.06% with signal high-pass filtered at 10Hz).

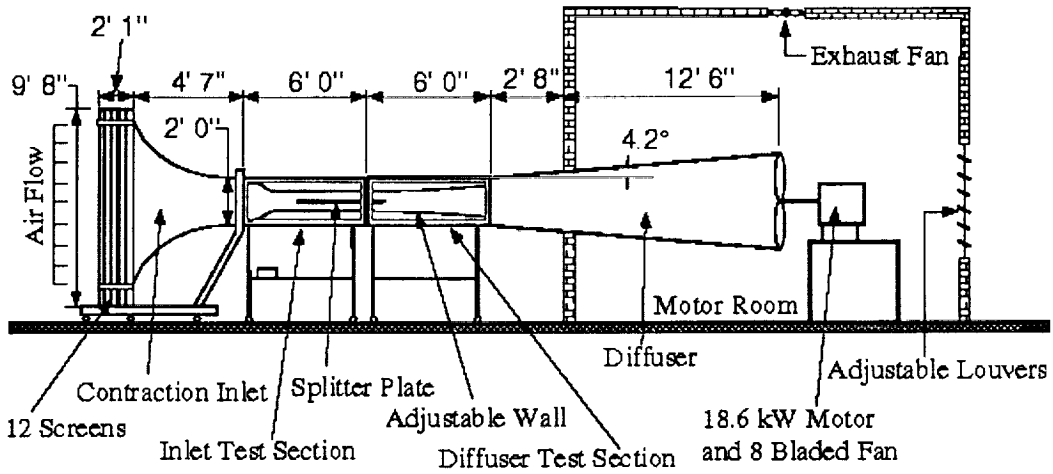

Figure 1. Schematic of the Notre Dame Subsonic Wind Tunnel and Wake Test Section.

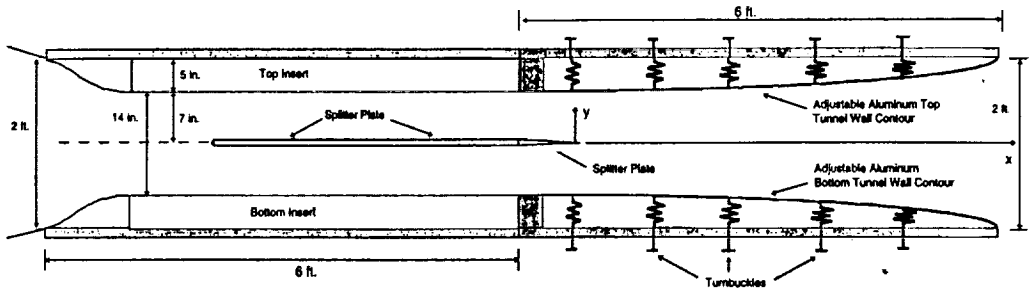

Figure 2. Schematic of the Test Section.

The wind tunnel consists of two consecutive test sections, the inlet test section and the diffuser test section, both of which were specifically constructed for the wake development experiment, as shown in Figure 1. The inlet test section is 6 ft. in length, 2 ft. in width and 14 inches in height. The length and the width of the diffuser test section are the same as those of the inlet test section while both the top and bottom walls of the diffuser test section were adjustable in order to create a pressure gradient environment. The top and bottom walls of the diffuser test section were made of sheet metal and their contour is adjustable by means of seven groups of turnbuckles. In this manner, the contour could be optimized to produce a desired constant pressure gradient environment. To facilitate flow visualization and LDV measurement, both the inlet and the diffuser test

sections have a sidewall made of glass. A schematic of the test sections is given in Figure 2.

3.1.2 Splitter Plate

The wake generating body is a two-dimensional splitter plate with round nose and tapered trailing edge, as illustrated in Figure 3. The chord length of the flat plate is 4 feet. The plate has multiple surface pressure taps and their associated internal tubing. The model is sidewall mounted with end plates used to minimize the influence of tunnel sidewall boundary layers. The boundary layer on the plate was artificially tripped by distributed roughness over the nose.

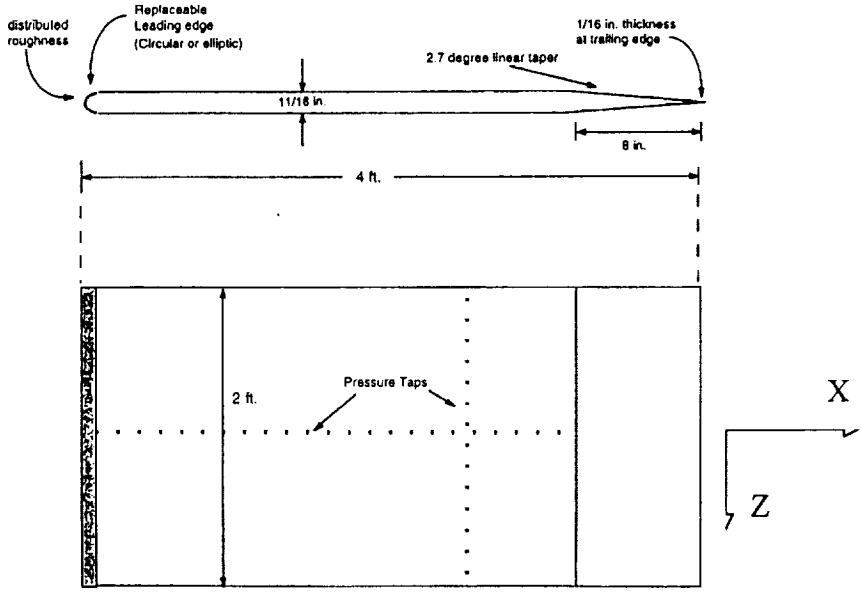

(Note: The drawing is not to scale)

Figure 3. Splitter Plate Geometry.

Before the detailed wake investigation was conducted, surface pressure distributions and boundary layer profiles on the splitter plate were first documented. These results can be found in the Year One Report or AIAA paper 99-0677.

3.2 Imposed Pressure Distribution

The experimental investigation was conducted in the diffuser test section, which is located immediately downstream of the splitter plate and, with adjustable top and bottom walls, is used to produce the desired adverse/favorable pressure gradient environment for wake development. The adjustment of the wall contour is achieved by turning seven groups of turnbuckles, as shown in Figure 2.

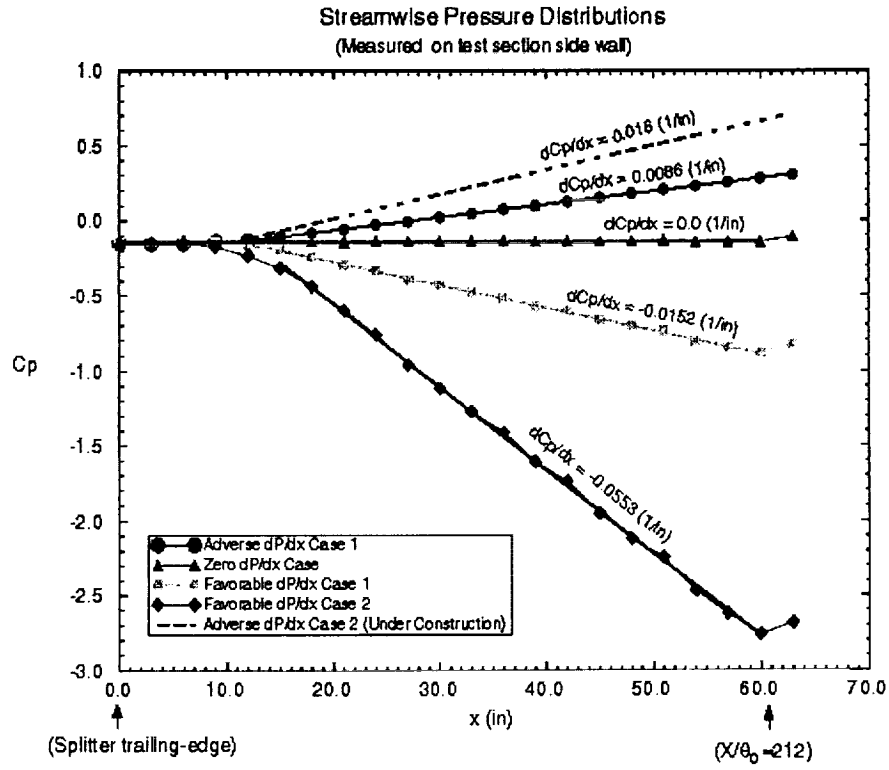

Figure 4. Experimentally Measured Pressure Distributions of Zero, Adverse and Favorable Pressure Gradient Cases.

Three sets of turbulent kinetic energy budget experiments were conducted for the symmetric wake: 1) zero pressure gradient (abbreviated as ZPG, base flow, dCp/dx = 0.0/inch); 2) moderate adverse pressure gradient (abbreviated as APG, dCp/dx = 0.0086/inch) and 3) moderate favorable pressure gradient (abbreviated as FPG, dCp/dx = -0.0152/inch). The measured streamwise pressure distributions corresponding to these different experimental sets are shown in Figure 4. These pressure distributions were measured by taps located on the sidewall of the diffuser test section at the same lateral (i.e. y) location as the centerline of the wake. LDV-based $U_e(x)$ measurements were found to be consistent with the measured wall pressure variation confirming the suitability of the pressure tap placement. Figure 4 also shows stronger favorable and adverse pressure gradients for which the TKE budget measurement were not performed.

Note that in each case, a zero pressure gradient zone was deliberately left at the beginning portion of the flow field to ensure that the wake initial condition is identical in each case. In Figure 4 the pressure coefficient Cp is defined as:

$$C_p = \frac{p - p_\infty}{p_0 - p_\infty}$$

where p is the static pressure measured at the pressure tap, p_0 and p_∞ are total and static pressures measured by a Pitot-static tube which is placed 4 inch upstream of the leading edge of the splitter plate.

3.3 Flow Parameters

The experiments were run at a Reynolds number Re of 2.4×10^6 (based on the chord length of splitter plate and a free stream velocity of 30.0 m/s) for all ZPG, APG and FPG cases. As a basis for comparison, it may be noted that a Boeing 737-100 operating at a wing chord Reynolds number of 15.7×10^6 during landing approach will have a slat Reynolds number of only about 1.8×10^6.

For the ZPG, APG and FPG cases, which have the same tunnel speed of 30m/s, the initial wake momentum thickness θ_0 = 7.2 mm. The Reynolds number Re_θ based on the initial wake momentum thickness θ_0 is 1.5×10^4.

This study focuses on near wake behavior due to its relevance for high-lift applications. From Figure 4, it can be seen that the useful length of the test section for the investigation of the wake development spans 60 inches downstream of the trailing edge of the splitter plate. This streamwise range corresponds to $0 < x/\theta_0 < 212$ for the symmetric wake development. The TKE measurements were made at the center span location for a variety of streamwise locations within the aforementioned range of the diffuser test section.

3.4 Experimental Apparatus used for the TKE Budget Measurement

From equation (6), it can be seen that the estimate of TKE budget requires the measurement of all three fluctuating velocity components of the turbulent flow. According to many references, such as Meyers[21] (1985), LDV is not a reliable tool for the spanwise velocity component measurement since there is usually a considerable uncertainty associated with the measurement of this quantity by using LDV. In addition, using LDV would confront with considerable difficulty in the dissipation term estimate since LDV relies on the random arrival of particles and the sampling frequency is not controllable. To ensure the accuracy of the TKE budget measurement, unlike the whole flow field LDV survey during year-one and year-two studies, this time we use only the constant temperature hot wire anemometry (CTA) technique to conduct the TKE budget measurement.

In the year-three study, a multi-channel TSI IFA 100 anemometer together with X-wire probes (Auspex type AHWX-100) and a dual parallel sensor probe (Auspex type AHWG-100) were used for the TKE budget measurement. The wires of the above probes are made of tungsten with the diameter of 5μm. The distance between the tip of the X-wire prongs is about 1.2mm. The spacing between the dual sensors of the parallel probe is 0.3mm. The length of the parallel probe sensor is around 0.9mm. As a comparison, the Kolmogorov microscale L_K ($L_K = (\nu/\varepsilon)^{1/4}$) of the wake flows is around 0.1mm. The anemometer output is anti-alias filtered at 20 kHz and digitally sampled at 40 kHz. The 20kHz Niquist frequency is chosen to correspond approximately to the Kolmogorov frequency, f_K ($f_K = U/2\pi L_K$) of the flow at the center of wake. The total record length at each measurement point is 13.1 seconds. The 40 kHz sampling frequency location

corresponds to the k^{-7} law zone in the frequency spectrum for the wake flow, as shown in Figure 5, suggesting the whole inertial sub-range is covered in the measurement.

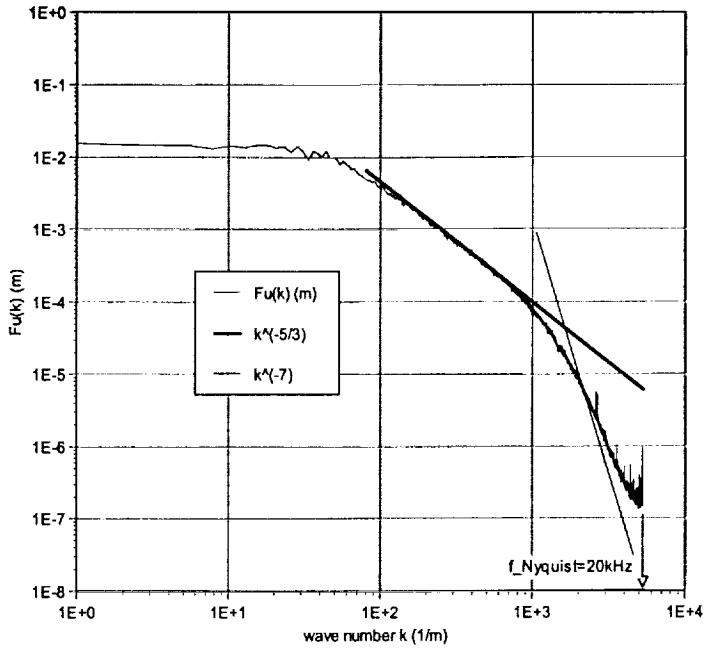

Figure 5. Typical Spectrum of the u-component for Symmetric Wake at APG.

To fulfill the dissipation measurement requirement based on the locally axisymmetric homogeneous turbulence assumption, a twin X-wire probe configuration was used for the fluctuation velocity derivative measurement, as shown in Figure 6. In fact, this twin X-wire configuration is primarily designed for the mean-square derivative $\overline{\left(\frac{\partial u_2'}{\partial x_3}\right)^2}$ measurement, which cannot be obtained by using a single X-wire probe.

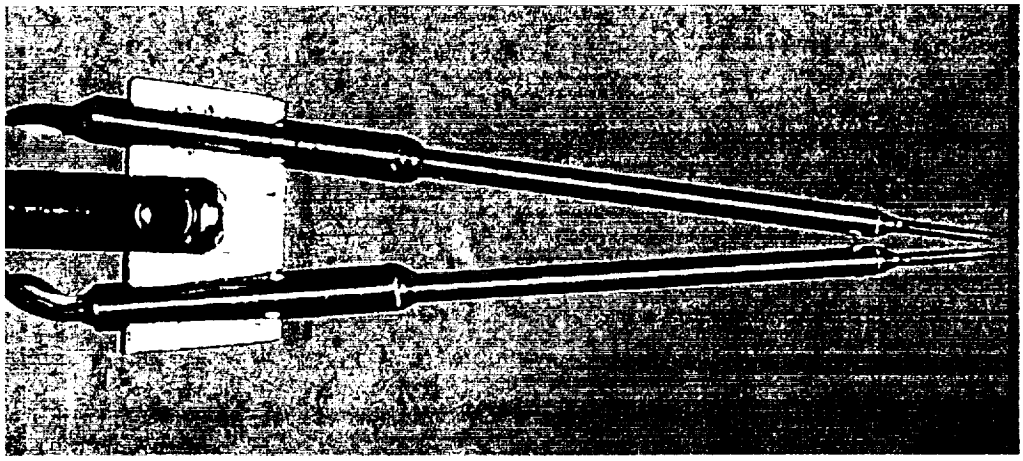

Figure 6. Twin X-wire Probe Configuration for Dissipation Measurement.

3.5 TKE Budget Measurement Scheme

To obtain the streamwise derivatives that are essential for the TKE budget estimate, we need to conduct lateral traverse at three consecutive streamwise measurement stations. The spatial derivatives can then be estimated as finite differences of the data taken at these streamwise separated nodal points. For example, suppose we want to estimate the TKE budget at station i, as shown in Figure 7, we need to conduct the lateral traverse not only at station i, but also at stations i+1 and i-1 as well. More specifically, to estimate the TKE budget at station i, we need a total of eight different traverses at stations i, i-1 and i+1, respectively. The quantities measured during each traverse are outlined below.

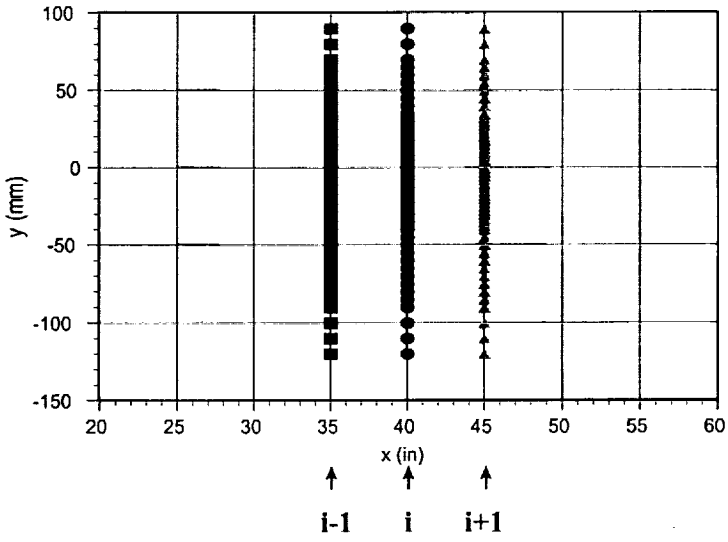

Figure 7. Schematic of Measuring Nodal Points.

- Traverse I: At station i, conduct the lateral traverse of the *twin X-wire configuration* to get $\overline{U_1}$, $\overline{U_2}$ $\overline{u_1'^2}$, $\overline{u_2'^2}$, $\overline{u_1'^3}$ $\overline{u_1'u_2'^2}$, $\overline{u_1'^2u_2'}$. $\overline{\left(\frac{\partial u_1'}{\partial x_3}\right)^2}$, $\overline{\left(\frac{\partial u_2'}{\partial x_3}\right)^2}$, $\overline{\left(\frac{\partial u_1'}{\partial x_1}\right)^2}_A$, $\overline{\left(\frac{\partial u_2'}{\partial x_1}\right)^2}_A$, $\overline{\left(\frac{\partial u_1'}{\partial x_1}\right)^2}_B$ and $\overline{\left(\frac{\partial u_2'}{\partial x_1}\right)^2}_B$, where the subscription A and B denote the quantity obtianed by X-wire A and B of the twin. The orietation of the twin X-wire at this traverse is equivalent to the one specified in Figure 1(d) of Browne, Antonia and Shah[11] (1987).
- Traverse II: At station i, rotate the *twin X-wire configuration* and conduct the lateral traverse to get $\overline{U_1}$, $\overline{U_3}$ $\overline{u_1'^2}$, $\overline{u_3'^2}$, $\overline{u_1'^3}$, $\overline{u_1'u_3'^2}$ $\overline{\left(\frac{\partial u_1'}{\partial x_2}\right)^2}$, $\overline{\left(\frac{\partial u_3'}{\partial x_2}\right)^2}$, $\overline{\left(\frac{\partial u_1'}{\partial x_1}\right)^2}_A$, $\overline{\left(\frac{\partial u_3'}{\partial x_1}\right)^2}_A$, $\overline{\left(\frac{\partial u_1'}{\partial x_1}\right)^2}_B$ and $\overline{\left(\frac{\partial u_3'}{\partial x_1}\right)^2}_B$, The orietation of the twin X-wire at this traverse is equivalent to the one specified in Figure 1(b) of Browne, Antonia and Shah[11] (1987).

- Traverse III: At station i, conduct the *parallel probe* lateral traverse to get $\overline{\left(\frac{\partial u_1'}{\partial x_2}\right)^2}$ and $\overline{\left(\frac{\partial u_1'}{\partial x_1}\right)^2}_A$ and $\overline{\left(\frac{\partial u_1'}{\partial x_1}\right)^2}_B$.
- Traverse IV: At station i, rotate the *parallel probe* and conduct the lateral traverse to get $\overline{\left(\frac{\partial u_1'}{\partial x_3}\right)^2}$ and $\overline{\left(\frac{\partial u_1'}{\partial x_1}\right)^2}_A$ and $\overline{\left(\frac{\partial u_1'}{\partial x_1}\right)^2}_B$.
- Traverse V: At station i+1 (Δx=5in), conduct the lateral traverse of the *single X-wire* to get $\overline{U_1}$, $\overline{U_2}$ $\overline{u_1'^2}$, $\overline{u_2'^2}$, $\overline{u_1'^3}$ $\overline{u_1'u_2'^2}$ and $\overline{u_1'^2u_2'}$.
- Traverse VI: At station i+1 (Δx=5in), rotate the *single X-wire* and conduct the lateral traverse to get $\overline{U_1}$, $\overline{U_3}$ $\overline{u_1'^2}$, $\overline{u_3'^2}$, $\overline{u_1'^3}$ and $\overline{u_1'u_3'^2}$.
- Traverse VII: At station i-1 (Δx=5in), conduct the lateral traverse of the *single X-wire* to get $\overline{U_1}$, $\overline{U_2}$ $\overline{u_1'^2}$, $\overline{u_2'^2}$, $\overline{u_1'^3}$ $\overline{u_1'u_2'^2}$ and $\overline{u_1'^2u_2'}$.
- Traverse VIII: At station i-1 (Δx=5in), rotate the *single X-wire* and conduct the lateral traverse to get $\overline{U_1}$, $\overline{U_3}$ $\overline{u_1'^2}$, $\overline{u_3'^2}$, $\overline{u_1'^3}$ and $\overline{u_1'u_3'^2}$.

The convection terms of the TKE budget can be estimated from the data taken at Traverses I and II. The turbulence diffusion terms from Traverses I, II, V, VI, VII and VIII. The production terms from the data taken at Traverses I, V and VII. The dissipation terms from Traverses I, II, III and IV. Appropriate piece-wise curve-fitting methods were used in order to obtain a smooth curve for the estimation of derivatives.

4. EXPERIMENTAL RESULTS AND DISCUSSION

4.1 Wake Flow Nomenclature

Figure 8 presents key nomenclature that will be used in characterizing the mean flow development of the wake. In the discussion to follow, $u_d(x, y)$ will be used to denote the local wake velocity defect while $U_d(x)$ will denote the maximum local velocity defect in the wake, as illustrated in Figure 8. The wake half-width, corresponding to the lateral distance from the centerline of the wake to the 50% maximum velocity defect location, is denoted as $\delta(x)$. The origin of the x-y coordinates of the flow field in the diffuser test section is located at the trailing edge of the splitter plate.

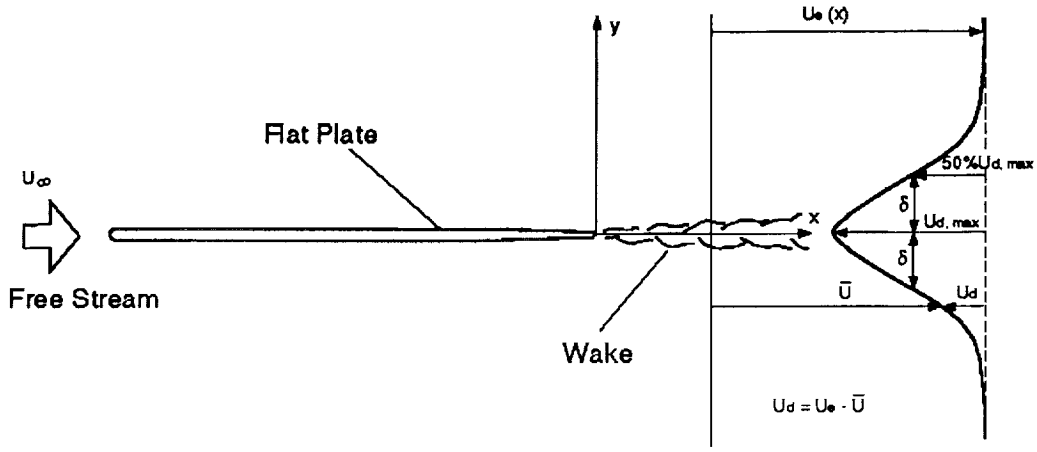

Figure 8. Wake Structure Nomenclature.

4.2 Turbulent Kinetic Energy Budget in Zero Pressure Gradient

To facilitate the interpretation of the TKE budget measurement result, we move the convection term $\overline{U_1}\frac{\partial}{\partial x_1}\left(\frac{\overline{q^2}}{2}\right)+\overline{U_2}\frac{\partial}{\partial x_2}\left(\frac{\overline{q^2}}{2}\right)$ in Equation (6) to the right hand side of the equation so that the TKE conservation equation reads

$$0 = \underbrace{-\overline{U_1}\frac{\partial}{\partial x_1}\left(\frac{\overline{q^2}}{2}\right)-\overline{U_2}\frac{\partial}{\partial x_2}\left(\frac{\overline{q^2}}{2}\right)}_{\text{Convection}}$$

$$\underbrace{-\frac{\partial}{\partial x_1}\overline{u_1'\frac{p'}{\rho}}-\frac{\partial}{\partial x_2}\overline{u_2'\frac{p'}{\rho}}}_{\text{Pressure Transport}} \quad \underbrace{-\frac{\partial}{\partial x_1}\overline{\frac{1}{2}\left(u_1'^3+u_1'u_2'^2+u_1'u_3'^2\right)}-\frac{\partial}{\partial x_2}\overline{\frac{1}{2}\left(u_1'^2u_2'+u_2'^3+u_2'u_3'^2\right)}}_{\text{Turbulence Diffusion}}$$

$$\underbrace{-\left(\overline{u_1'^2}-\overline{u_2'^2}\right)\frac{\partial\overline{U_1}}{\partial x_1}-\overline{u_1'u_2'}\left(\frac{\partial\overline{U_1}}{\partial x_2}+\frac{\partial\overline{U_2}}{\partial x_1}\right)}_{\text{Production}} \quad \underbrace{+\frac{\nu}{2}\frac{\partial^2\overline{q^2}}{\partial x_1^2}+\frac{\nu}{2}\frac{\partial^2\overline{q^2}}{\partial x_2^2}}_{\text{Viscous Diffusion}}$$

$$\underbrace{-\nu\left(\overline{\left(\frac{\partial u_1'}{\partial x_1}\right)^2}+\overline{\left(\frac{\partial u_1'}{\partial x_2}\right)^2}+\overline{\left(\frac{\partial u_1'}{\partial x_3}\right)^2}+\overline{\left(\frac{\partial u_2'}{\partial x_1}\right)^2}+\overline{\left(\frac{\partial u_2'}{\partial x_2}\right)^2}+\overline{\left(\frac{\partial u_2'}{\partial x_3}\right)^2}+\overline{\left(\frac{\partial u_3'}{\partial x_1}\right)^2}+\overline{\left(\frac{\partial u_3'}{\partial x_2}\right)^2}+\overline{\left(\frac{\partial u_3'}{\partial x_3}\right)^2}\right)}_{\text{Dissipation}} \qquad (19)$$

In the following discussions, the term convection will refer to the one in Equation (19).

4.2.1 Convection Term

The convection term $-\overline{U_1}\frac{\partial}{\partial x_1}\left(\frac{\overline{q^2}}{2}\right)-\overline{U_2}\frac{\partial}{\partial x_2}\left(\frac{\overline{q^2}}{2}\right)$ consists of two parts, the streamwise convection $-\overline{U_1}\frac{\partial}{\partial x_1}\left(\frac{\overline{q^2}}{2}\right)$ and the lateral convection $-\overline{U_2}\frac{\partial}{\partial x_2}\left(\frac{\overline{q^2}}{2}\right)$. These terms can be

measured directly. The lateral distribution of these two terms for the symetric wake at ZPG at x/θ_0 =141 is presented in Figure 9. In this figure the convection terms are non-dimensionalized by using the local wake half-width δ as the reference length scale and the local maximum velocity defect U_d as the reference velocity scale. From this figure, it can be seen that for the symetric wake in ZPG, the streamwise convection dominates in the total convection disdtribution.

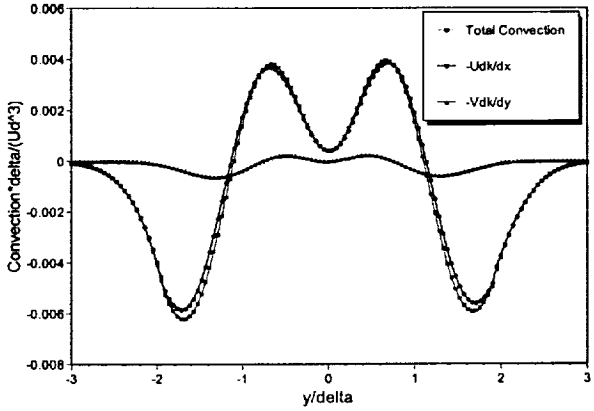

Figure 9. Convection Term of Symmetric Wake at ZPG at x/θ_0 =141.

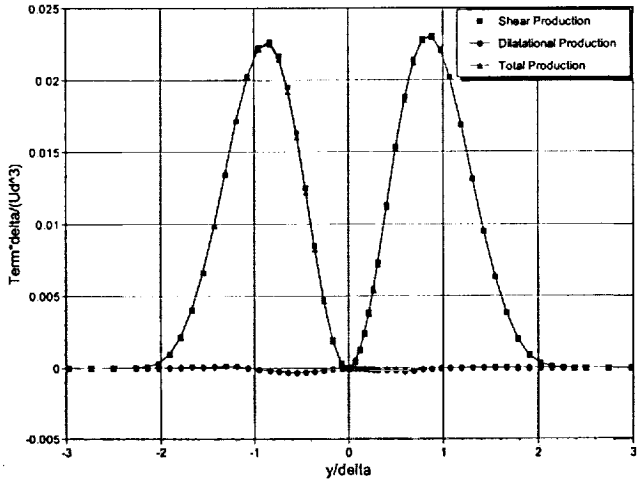

Figure 10. Production Term of Symmetric Wake at x/θ_0 =141.

4.2.2 Production Term

The turbulence production term $-\left(\overline{u_1'^2}-\overline{u_2'^2}\right)\frac{\partial \overline{U_1}}{\partial x_1}-\overline{u_1'u_2'}\left(\frac{\partial \overline{U_1}}{\partial x_2}+\frac{\partial \overline{U_2}}{\partial x_1}\right)$ consists of two parts, the shear production term $-\overline{u_1'u_2'}\left(\frac{\partial \overline{U_1}}{\partial x_2}+\frac{\partial \overline{U_2}}{\partial x_1}\right)$ and the dilatational production term $-\left(\overline{u_1'^2}-\overline{u_2'^2}\right)\frac{\partial \overline{U_1}}{\partial x_1}$. These terms are measured directly. Figure 10 compares these production terms for the symmetric wake at ZPG at x/θ_0 = 141. This figure clearly shows that the wake flow at

zero pressure gradient is shear dominated and the dilatational production is approximately zero, just as expected. In fact, for the wake flow at zero pressure gradient, $-\left(\overline{u_1'^2}-\overline{u_2'^2}\right)\frac{\partial \overline{U_1}}{\partial x_1}-\overline{u_1'u_2'}\left(\frac{\partial \overline{U_1}}{\partial x_2}+\frac{\partial \overline{U_2}}{\partial x_1}\right)\approx -\overline{u_1'u_2'}\frac{\partial \overline{U_1}}{\partial x_2}$ since $\frac{\partial \overline{U_1}}{\partial x_1}\approx 0$ and $\frac{\partial \overline{U_2}}{\partial x_1}\approx 0$. The same result was obtained during the year one investigation of the symmetric wake by using LDV, as presented in the Year-One Report.

4.2.3 Turbulent Diffusion Term

The turbulent diffusion term $-\frac{\partial}{\partial x_1}\overline{\frac{1}{2}\left(u_1'^3+u_1'u_2'^2+u_1'u_3'^2\right)}-\frac{\partial}{\partial x_2}\overline{\frac{1}{2}\left(u_1'^2u_2'+u_2'^3+u_2'u_3'^2\right)}$ is composed of two parts, the streamwise turbulent diffusion $-\frac{\partial}{\partial x_1}\overline{\frac{1}{2}\left(u_1'^3+u_1'u_2'^2+u_1'u_3'^2\right)}$ and the lateral turbulent diffusion $-\frac{\partial}{\partial x_2}\overline{\frac{1}{2}\left(u_1'^2u_2'+u_2'^3+u_2'u_3'^2\right)}$. Figure 11 shows the profile of these diffusion terms for the symmetric wake at ZPG at $x/\theta_0 = 141$. It can be seen that obviously, for the wake at zero pressure gradient, the lateral turbulent diffusion is the dominant turbulent diffusion mechanism and the streamwise turbulent diffusion is negligible. To verify the accuracy of the measurement of the diffusion term, the profile of the total turbulent diffusion term is integrated along the lateral direction across wake. The integration result is essentially zero, as one would expect, since lateral diffusion serves only to redistribute turbulent kinetic energy. This result can also be viewed as an indication of the accuracy of the diffusion term measurement.

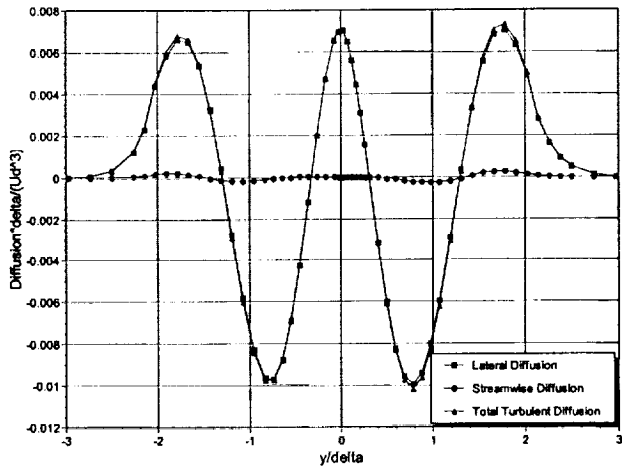

Figure 11. Turbulent Diffusion Term of Symmetric Wake at ZPG at x/θ_0 =141.

4.2.4 Dissipation Term

Following the TKE measurement scheme outlined in Section 3.5, we were able to obtain a comprehensive set of data which allow us to estimate the dissipation term in four different approaches, namely, (a), the isotropic turbulence assumption approach, (b), the

locally axisymmetric turbulence assumption approach, (c), the semi-isotropic assumption approach and (d) the forced TKE balance approach, as described in Section 2.2. The methodology of these approaches and the corresponding results will be presented in the following subsections, repectively.

4.2.4.1 Dissipation Based on Isotropic Turbulence Assumption

The approach based on the isotropic turbulence assumption requires the estimate of the mean square derivative term $\overline{\left(\frac{\partial u_1'}{\partial x_1}\right)^2}$, which can be obtained from data series measured in Traverse I, II, III and IV by invoking the Taylor's frozen field hypothesis $\frac{\partial}{\partial x} \approx -\frac{1}{U_1}\frac{\partial}{\partial t}$. All restults obtained in Travese I to IV using X-wire and parallel probes for the quantity $\overline{\left(\frac{\partial u_1'}{\partial x_1}\right)^2}$ at ZPG are shown in Figure 12.

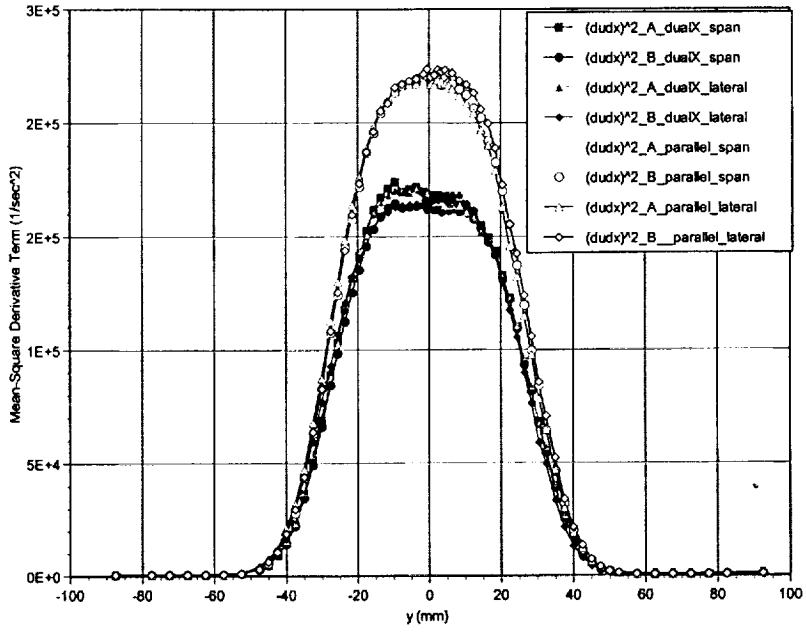

Figure 12. Comparison of $\overline{\left(\frac{\partial u_1'}{\partial x_1}\right)^2}$ measured by X-wire and parallel probes at ZPG at x/θ_0 =141.

From Figure 12, it can be seen that the parallel probe gives higher measurement values for the quantity $\overline{\left(\frac{\partial u_1'}{\partial x_1}\right)^2}$ than the X-wire probe. This disparity can be attributed to the difference between the effective sensing length of the wires on the parallel and the X-wire probes. The length of the sensors on the parallel probe is only 0.9mm while the distance between the tip of the X-wire prongs is about 1.2mm. According to Wallace and Foss[22] (1995), the sensing length of the probe is crucial for the measurement of the mean-

square derivatives such as for the quantity $\overline{\left(\frac{\partial u_1'}{\partial x_1}\right)^2}$. Usually a longer wire gives rise to smaller magnitude of the mean-square derivative measurement due to spatial filtering, which is exactly the case in Figure 12. Thus the quanty $\overline{\left(\frac{\partial u_1'}{\partial x_1}\right)^2}$ measured by using the paralle probe is likely to be closer to the true value of $\overline{\left(\frac{\partial u_1'}{\partial x_1}\right)^2}$ compared to the X-wire measurement. This was one of the motivations for using the parallel probe results for the dissipation estimates. The dissipation estimate for the ZPG case based on the isotropic turbulence assumption is presented in Figure 13. This figure also presents dissipation estimates based on other approaches for direct comparison. The discussion of the comparison of the the dissipation estimate with different appraoches can be found in Section 4.2.4.5.

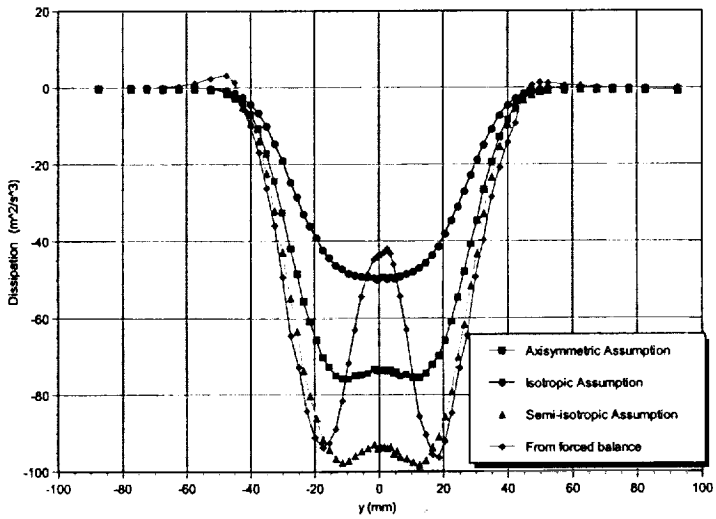

Figure 13. Comparison of dissipation estimate with different approaches for ZPG at x/θ_0 =141.

4.2.4.2 Dissipation Based on Locally Axisymmetric Turbulence Assumption

As described in Section 2.2, as long as the turbulence field satisfies the conditions set forth in Equations (9)-(15), the dissipation term can be estimated via the so-called locally axisymmetric turbulence assumption, which, as shown in Equation (16), requires the measurement of four mean-square derivatives $\overline{\left(\frac{\partial u_1'}{\partial x_1}\right)^2}$, $\overline{\left(\frac{\partial u_1'}{\partial x_3}\right)^2}$, $\overline{\left(\frac{\partial u_2'}{\partial x_1}\right)^2}$ and $\overline{\left(\frac{\partial u_2'}{\partial x_3}\right)^2}$. The verification of the prerequisites for the application of the locally axisymmetric turbulence assumption will be discussed in Section 4.2.4.6. In the following paragraphs, the methodology for the determination of the four mean-square derivatives will be discussed and the results will be presented.

First, the determination of the mean-square derivative $\overline{\left(\frac{\partial u_1'}{\partial x_1}\right)^2}$ has been described in Section 4.2.4.1, and as in the isotropic assumption approach, this mean-square derivative is measured with the parallel probe.

Secondly, as described in Section 3.5, both Traverse I (twin X-wire configuration) and Traverse IV(parallel probe) can provide the mean-square derivative $\overline{\left(\frac{\partial u_1'}{\partial x_3}\right)^2}$. The comparison of the measured profile of the the mean-square derivative $\overline{\left(\frac{\partial u_1'}{\partial x_3}\right)^2}$ by the twin X-wire configuration and the parallel probe is shown in Figure 14. Again, as was the case for the $\overline{\left(\frac{\partial u_1'}{\partial x_1}\right)^2}$ measurement, the parallel probe yield a higher magnitude of the quantity. The much smaller magnitude of $\overline{\left(\frac{\partial u_1'}{\partial x_3}\right)^2}$ measured by the twin X-wire configuration is primarily due to the poor spatial resolution of the twin X-wire configuration. Obviously, the mean-square derivative $\overline{\left(\frac{\partial u_1'}{\partial x_3}\right)^2}$ measured by the parallel probe is closer to the true value and therefore is used for the dissipation estimate.

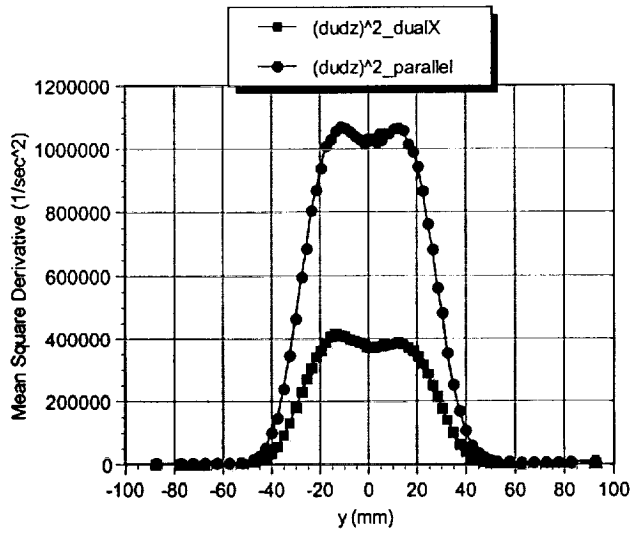

Figure 14. Comparison of $\overline{\left(\frac{\partial u_1'}{\partial x_3}\right)^2}$ measured by twin X-wire and parallel probes at ZPG at x/θ_0 =141.

The mean-square derivative $\overline{\left(\frac{\partial u_2'}{\partial x_1}\right)^2}$ can be obtained from an X-wire in Traverse I by invloking the Taylor's frozen field hypothesis. As is known from the discussion in Section 4.2.4.1, the quantity $\overline{\left(\frac{\partial u_1'}{\partial x_1}\right)^2}$ obtained by the X-wire is smaller than its counterpart obtained by the parallel probe due the relatively larger size of the X-wire probe. Similary,

it is reasonable to assume that the quantity $\overline{\left(\frac{\partial u_2'}{\partial x_1}\right)^2}$ measured by the X-wire is also reduced in magnitude at the same rate as the quantity $\overline{\left(\frac{\partial u_1'}{\partial x_1}\right)^2}$, if compared with a parallel probe measurement. With this assumption, one can obtain a correction coefficient from Figure 12, which is nothing but the ratio between $\overline{\left(\frac{\partial u_1'}{\partial x_1}\right)^2}$_parallel probe and $\overline{\left(\frac{\partial u_1'}{\partial x_1}\right)^2}$_X-wire and then apply this correction coefficient to $\overline{\left(\frac{\partial u_2'}{\partial x_1}\right)^2}$ to improve the accuracy of the measureemnt. That is the method we used for the quantity $\overline{\left(\frac{\partial u_2'}{\partial x_1}\right)^2}$, which is invloved in the final dissipation estimate.

The quantity $\overline{\left(\frac{\partial u_2'}{\partial x_3}\right)^2}$ can only be obtained from the twin X-wire configuration measureement in Traverse I. In fact, as mentioned in Section 3.4, this twin X-wire configuration is primarily designed for the mean-square derivative $\overline{\left(\frac{\partial u_2'}{\partial x_3}\right)^2}$ measurement. As was the case for the quantity $\overline{\left(\frac{\partial u_1'}{\partial x_3}\right)^2}$ shown in Figure 14, it is reasonable to assume that the quantity $\overline{\left(\frac{\partial u_2'}{\partial x_3}\right)^2}$ measured by the twin X-wire configuration is also reduced in magnitude at the same rate as the quantity $\overline{\left(\frac{\partial u_1'}{\partial x_3}\right)^2}$, if compared with a parallel probe measurement. With this assumption, we can obtain a correction coefficient from Figure 14, which is nothing but the ratio between $\overline{\left(\frac{\partial u_1'}{\partial x_3}\right)^2}$_parallel probe and $\overline{\left(\frac{\partial u_1'}{\partial x_3}\right)^2}$_twin-X-wire and then, apply this correction coefficient to $\overline{\left(\frac{\partial u_1'}{\partial x_3}\right)^2}$ to improve the accuracy of the measureemnt, just like the treatment to $\overline{\left(\frac{\partial u_2'}{\partial x_1}\right)^2}$ that we discussued in the above paragraph. The quantity $\overline{\left(\frac{\partial u_1'}{\partial x_3}\right)^2}$ invloved in the final dissipation estimate was corrected by this mehtod.

Finally, after all four mean-square derivatives $\overline{\left(\frac{\partial u_1'}{\partial x_1}\right)^2}$, $\overline{\left(\frac{\partial u_1'}{\partial x_3}\right)^2}$, $\overline{\left(\frac{\partial u_2'}{\partial x_1}\right)^2}$ and $\overline{\left(\frac{\partial u_2'}{\partial x_3}\right)^2}$ are appropriately treated, we can use Equation (16) to estimate the dissipation term based on the locally axisymmetric homogeneous turbulence assumption, the result of which is shown in Figure 13.

4.2.4.3 Dissipation Based on Semi-isotropic Turbulence Assumption

As described in Section 2.2, out of the nine fluctuating velocity derivatives appearing in the dissipation term in equation (4), the three streamwise mean-square derivatives $\overline{\left(\frac{\partial u_1'}{\partial x_1}\right)^2}$, $\overline{\left(\frac{\partial u_2'}{\partial x_1}\right)^2}$ and $\overline{\left(\frac{\partial u_3'}{\partial x_1}\right)^2}$ are estimated on the basis of parallel and X-wire measurements by invoking the Taylor's hypothesis in Traverse I, II, III and IV. The lateral and spanwise mean-square derivatives, $\overline{\left(\frac{\partial u_1'}{\partial x_2}\right)^2}$ and $\overline{\left(\frac{\partial u_1'}{\partial x_3}\right)^2}$ are obtained by a parallel hot-wire probe in Traverse III and IV. The two quantities $\overline{\left(\frac{\partial u_3'}{\partial x_2}\right)^2}$ and $\overline{\left(\frac{\partial u_2'}{\partial x_3}\right)^2}$ can be obtained by using the twin X-wire configuration in Tanverse I and II. In summary, only two out the nine derivatives in the dissipation term as shown in Equation (4), $\overline{\left(\frac{\partial u_2'}{\partial x_2}\right)^2}$ and $\overline{\left(\frac{\partial u_3'}{\partial x_3}\right)^2}$, have not been directly measured in this research project. The experimental results of these seven measured terms for the symmetric wake at zero pressure gradient at $x/\theta_0 = 141$ are shown in Figure 15. All time mean derivatives shown in Figure 15 have been corrected for the resolution bias error using the method descibed in the previous section. It can be seen, as shown in Figure 15, the streamwise derivatives are much smaller than the two lateral and spanwise fluctuating velocity derivatives.

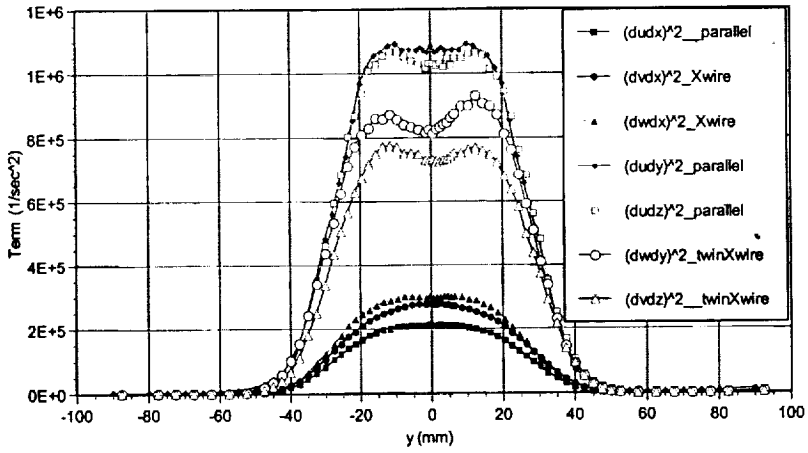

Figure 15. The Seven Measured Time Mean Square Derivatives at ZPG at $x/\theta_0 = 141$.

The two remaining derivatives $\overline{\left(\frac{\partial u_2'}{\partial x_2}\right)^2}$ and $\overline{\left(\frac{\partial u_3'}{\partial x_3}\right)^2}$ in the dissipation term are subsequently estimated by invoking a semi-isotropy assumption (Wygnanski and Fiedler[8] (1969)).

$$k_s\overline{\left(\frac{\partial u_1'}{\partial x_1}\right)^2} = \overline{\left(\frac{\partial u_2'}{\partial x_1}\right)^2} = \overline{\left(\frac{\partial u_3'}{\partial x_1}\right)^2}$$

$$\overline{\left(\frac{\partial u_1'}{\partial x_2}\right)^2} = k_s\overline{\left(\frac{\partial u_2'}{\partial x_2}\right)^2} = \overline{\left(\frac{\partial u_3'}{\partial x_2}\right)^2}$$

$$\overline{\left(\frac{\partial u_1'}{\partial x_3}\right)^2} = \overline{\left(\frac{\partial u_2'}{\partial x_3}\right)^2} = k_s\overline{\left(\frac{\partial u_3'}{\partial x_3}\right)^2}$$

where k_s is the semi-isotropy coefficient. To verify if the semi-isotropy assumption is valid for the wake flow investigated here, it can be seen from Figure 15, that $\overline{\left(\frac{\partial u_2'}{\partial x_1}\right)^2} \approx \overline{\left(\frac{\partial u_3'}{\partial x_1}\right)^2}$ which means the last equality in the first row of the semi-istropy assumption matrix is valid. From this figure, the semi-isotropy coefficient k_s can also been determined according to the assumption $k_s\overline{\left(\frac{\partial u_1'}{\partial x_1}\right)^2} = \overline{\left(\frac{\partial u_2'}{\partial x_1}\right)^2}$. With this experimentally determined semi-isotropy coefficient k_s, the remaining two derivatives $\overline{\left(\frac{\partial u_2'}{\partial x_2}\right)^2}$ and $\overline{\left(\frac{\partial u_3'}{\partial x_3}\right)^2}$ in the decipation term can then be estimated. Finally, the total dissipation can be calculated from Equation (4). The result of the dissipatio estimate obtained in this way is shown in Figure 13.

4.2.4.4 Dissipation Based on Forced TKE Balance

As outlined in Section 2.2, the dissipation term may even be inferred by a forced balance of the TKE equation, *if the pressure diffusion term can be neglected.* Actually, the dissipation term obtained with this forced balance method contains the pressure diffusion term and the error term. Again, the dissipation term obtained by forcing a balance of the TKE equation is shown in Figure 13.

4.2.4.5 Comparison of the Results of the Four Approaches

As shown in Figure 13, it can be seen that significant disparities occur for the estimates of the dissipation term through the four different approaches for the symmetric wake at ZPG. The dissipation term based on the isotropy assumption is much smaller in magnitude compared with the other three methods. In fact, the accuracy of the dissipation estimate can be examined by checking zero lateral integration character of the pressure diffusion term, which can be obtained from Equation (19) if convection, production, turbulent diffusion and the dissipation terms are all measured. It turns out that the dissipation estimate based on the locally axisymmetric assumption leads to a lateral integration of the pressure diffusion term that is approximately zero, which means the locally axisymmetric assumption approach is most appropriate for the dissipation estimate for the wake flow studied in this research project. The estimate based on the

semi-isotropy assumption over-estimated the dissipation while the estimate based on isotropy under-estimated the dissipation.

4.2.4.6 Verification of the Prerequisites of the Locally Turbulence Assumption

Some of the conditions for the locally axisymmetric homogeneous turbulence assumption as outlined in Equations (9)-(15) can be verified from Figure 15, in which, it can be seen that Equations (9) and (10) are almost perfectly valid, i.e., $\overline{\left(\frac{\partial u_1'}{\partial x_2}\right)^2} = \overline{\left(\frac{\partial u_1'}{\partial x_3}\right)^2}$ and $\overline{\left(\frac{\partial u_2'}{\partial x_1}\right)^2} = \overline{\left(\frac{\partial u_3'}{\partial x_1}\right)^2}$, while Equation (12) is approximately valid within the uncertainty of the measurement, $\overline{\left(\frac{\partial u_2'}{\partial x_3}\right)^2} \approx \overline{\left(\frac{\partial u_3'}{\partial x_2}\right)^2}$.

4.2.5 Turbulent Kinetic Energy Budget

Figure 16 presents all measured terms in Equation (19) of the turbulent kinetic energy budget for the symmetric wake at zero pressure gradient at $x/\theta_0 = 141$. In this plot, all terms except the pressure diffusion are obtained from direct measurement. Error bars associated with the measured terms based on an uncertainty analysis are also shown in this figure. The pressure diffusion profile shown in Figure 16 is obtained by forcing a balance of the TKE equation and it is actually a term that consists of both the true pressure diffusion and the total error of the whole measurement.

The double peaks of the production term approximately correspond to the locations of the maximum mean strain rate in the upper and lower shear layer of the wake. At the center or near the edges of the wake, where the mean shear is zero or asymptotically approaches zero, the production term is also zero. The peak of the production term implies that a large amount of turbulence is newly generated in that region. This means there is a gradient associated with the newly generated turbulence kinetic energy in the flow field. This gradient associated with the newly generated turbulence kinetic energy is mainly aligned in the lateral direction. Wherever there is a gradient, the diffusion mechanism will take part in and play a role. From Figure 15, it can be seen it is the turbulent diffusion that transports the turbulence kinetic energy away from the region with higher density of newly generated turbulence to the regions with less density of newly generated turbulence, such as the center and the edges of the wake. The direction of the turbulent diffusion is governed by the production mechanism, mainly in the lateral direction. (This explains why the lateral diffusion dominates while the streamwise diffusion is negligible. The behavior of the turbulent diffusion depends on the behavior of the turbulence production.) More specifically, the turbulent diffusion will transport turbulence away from the location of the maximum mean shear and move the turbulence toward the center and the edges of the wake. As a consequence, we see there are two valleys of loss of the turbulent kinetic energy due to the turbulent diffusion near the locations of maximum mean shear while there are three peaks of gain due to turbulent diffusion at the center and near both edges of the wake. The turbulent diffusion is a conservative process and the role it plays is merely to re-distribute the turbulence kinetic energy and make the turbulence field more and more homogenized.

From Figure 16 it can also be seen that the pressure diffusion plays about the same role as that of the turbulent diffusion in the balance of the turbulent kinetic energy budget. The pressure diffusion also transports the turbulence away from the region with higher density of newly generated turbulence kinetic energy. There is no evidence in Figure 16 that there is a so-called counter-gradient transport mechanism for the pressure diffusion term, as suggested by Demuren et al[23] (1996). Figure 16 also shows the magnitude of the pressure diffusion is quite considerable and is not a quantity that can be simply neglected.

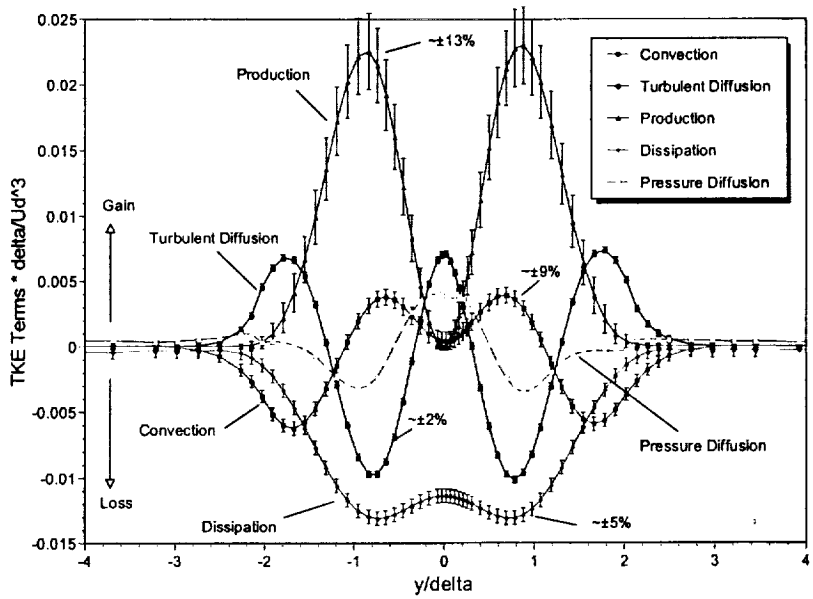

Figure 16. Turbulent Kinetic Energy Budget of Symmetric Wake at ZPG at x/θ_0 =141.

As for the dissipation term, it can be seen from Figure 16 that most severe dissipation occurs at the central region of the wake, where the turbulence is also most intense. Approaching to the edge of the wake, the dissipation gradually decreases to zero. Actually, at the central region of the wake, the dissipation is so intense that after the aggregation of the gain/loss of the turbulence kinetic energy due to production, turbulent diffusion, pressure diffusion and dissipation there is a deficit of the turbulence kinetic energy which requires the contribution from convection to make up the balance. In other words, without a gain of turbulent kinetic energy from the convection process, the whole system is unable to reach a local balance at the central region of the wake. This explains why we see a gain due to convection at the central region of the wake. As a contrast, near the edge of the wake, the dissipation turns to be so weak that it can only roughly balance the similarly weak production process and in the meanwhile, leave a considerable amount of gain of turbulence kinetic energy due to the diffusion process to be balanced by the loss carried out by the convection process. From this analysis, we can see that the role of convection in the turbulence kinetic energy budget balance largely depends on the behavior of the dissipation process.

In fact, the convection term can also be viewed as an interface, and actually, the only interface for the exchange of turbulence kinetic energy of the local TKE balance system with the upstream and downstream TKE balance systems, as shown in Figure 17.

Suppose there is a thin control volume, the thickness of which is dx, associated with the local TKE balance system. Obviously, k_{flux_in}, the turbulence kinetic energy flux from the upstream station is equal to the sum of the gain/loss of the turbulence kinetic energy of the local TKE balance system due to convection and k_{flux_out}, the turbulence kinetic energy flux to the downstream station. If there is a gain of the turbulence kinetic energy of the local TKE balance system due to convection, we should have, $k_{flux\_in} > k_{flux\_out}$, which implies that a decrease of the turbulence kinetic energy should be expected when the wake develops downstream. Similarly, if there is a loss of the turbulence kinetic energy of the local TKE balance system due to convection, we should have, $k_{flux\_in} < k_{flux\_out}$, which implies that an increase of the turbulence kinetic energy should be expected when the wake develops downstream.

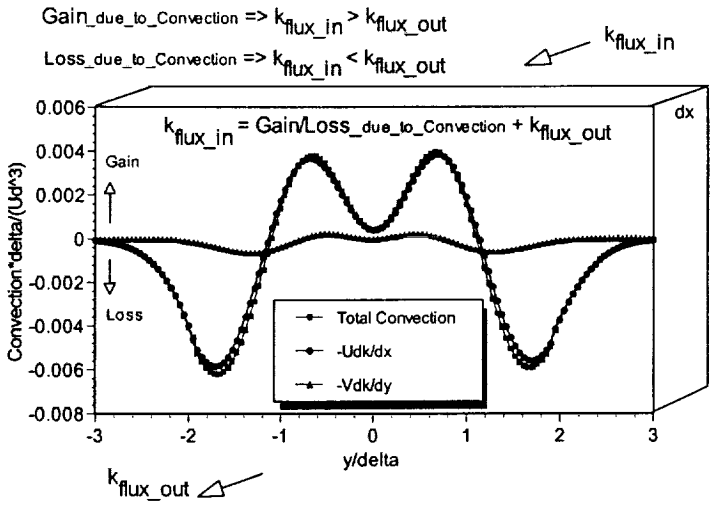

Figure 17. Relationship of Convection Term and the Turbulent Kinetic Energy Flux

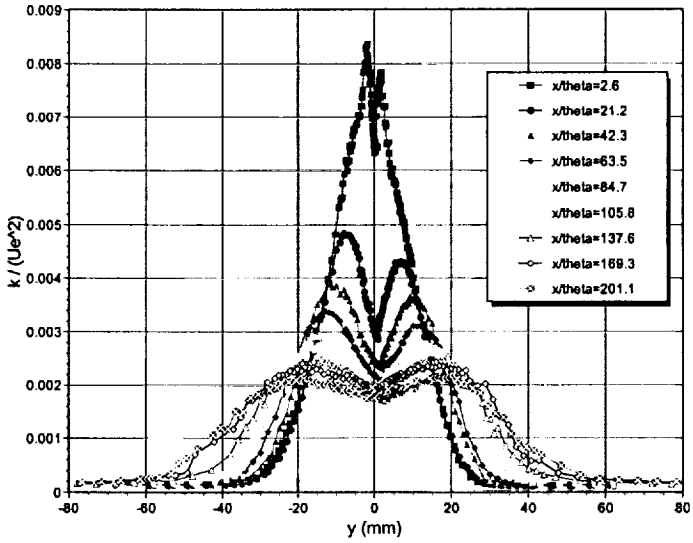

Figure 18. Streamwise Development of Turbulent Kinetic Energy of Symmetric Wake at ZPG

In fact, the convection term is nothing but a material derivative of the turbulence kinetic energy, as expressed in Equation (2), predicting whether the turbulence field will decay or grow in the downstream direction. As pointed out earlier, in Figure 16, near the center of the wake, there is a gain of TKE for the local system due to convection, indicating that the turbulence is decreasing near the center of the wake as the wake develops downstream. Again in Figure 16, at the edge of the wake, there is a loss of TKE for the local system due to convection, implying that the turbulence kinetic energy will increase at the edge of the wake. This trend can be found in Figure 18, which shows the streamwise development of the turbulence kinetic energy for the zero pressure gradient. Indeed, from Figure 18, one can clearly see that the turbulence kinetic energy is decreasing at the center of the wake while it is growing at the edge of the wake.

4.3 Turbulent Kinetic Energy Budget in Adverse Pressure Gradient

4.3.1 Convection Term

Figure 19 shows the measured convection term for the symmetric wake in adverse pressure gradient at $x/\theta_0 = 141$. Again, near the center of the wake, the streamwise convection $-\overline{U_1}\frac{\partial}{\partial x_1}\left(\frac{\overline{q^2}}{2}\right)$ dominates. However, unlike the ZPG case shown in Figure 8, the lateral convection $-\overline{U_2}\frac{\partial}{\partial x_2}\left(\frac{\overline{q^2}}{2}\right)$ is quite significant in magnitude near the edge of the wake for the APG case. This behavior is determined by the V-mean profile, which is shown in Figure 20 along with V-mean profiles for the ZPG and FPG cases. Figure 20 shows that for the APG case, the V velocity component grows in magnitude toward the edge of the wake. The V velocity component acts to convect turbulence kinetic energy toward the edge of the wake. That is why we that a gain of turbulence kinetic energy in this region. Like the ZPG case, the U-component still provides a gain of turbulence kinetic energy near the center and a loss at the edge of the wake. The competing gain and loss mechanism of the U and V component convection gives rise to a net loss of turbulence kinetic energy due to the total convection effect at the edge of the wake.

Figure 20 also shows that for the ZPG case, the magnitude of the V-mean profile is relatively much smaller across the wake than both APG and FPG cases. As a consequence, the lateral convection $-\overline{U_2}\frac{\partial}{\partial x_2}\left(\frac{\overline{q^2}}{2}\right)$ for the ZPG case is not as significnt as that of APG case near the edge of the wake. Since the sign of V-component at the FPG case is reversed from the APG case, it is expected that for the FPG case, the profile of the lateral convection $-\overline{U_2}\frac{\partial}{\partial x_2}\left(\frac{\overline{q^2}}{2}\right)$ will be an inverted version of the APG case. This will be shown in Figure 30.

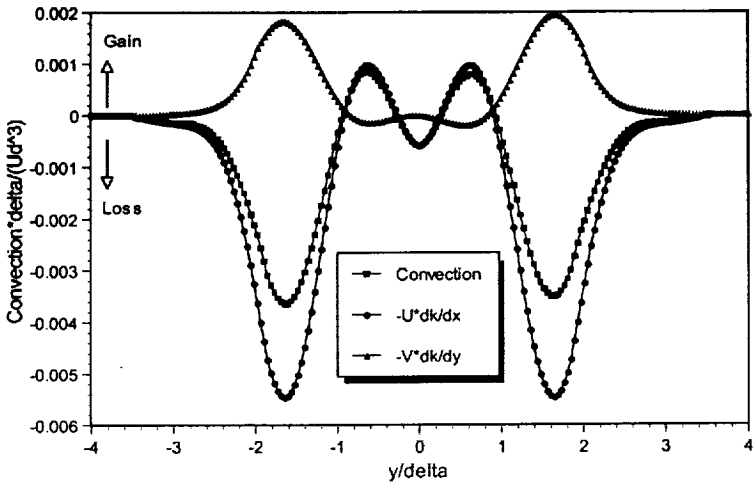

Figure 19. Convection Term of Symmetric Wake at APG at x/θ_0 =141.

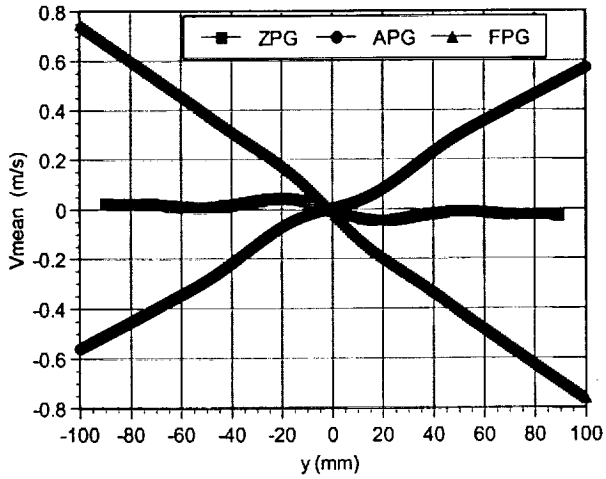

Figure 20. Comparison of the Vmean profiles for the Symmetric Wake ZPG, APG and FPG cases at x/θ_0 =141.

4.3.2 Production Term

Figure 21 shows the turbulence production of the symmetric wake at APG at x/θ_0 = 141. In this figure, the dilatational production refers to the $-\left(\overline{u_1'^2}-\overline{u_2'^2}\right)\frac{\partial \overline{U_1}}{\partial x_1}$ term. The shear production refers to the $-\overline{u_1'u_2'}\left(\frac{\partial \overline{U_1}}{\partial x_2}+\frac{\partial \overline{U_2}}{\partial x_1}\right)$ term. The shear production part 1 refers to the $-\overline{u_1'u_2'}\frac{\partial \overline{U_1}}{\partial x_2}$ term. The shear production part 2 refers to the $-\overline{u_1'u_2'}\frac{\partial \overline{U_2}}{\partial x_1}$ term. This figure shows that like the ZPG case, the wake flow in APG case investigated remains shear dominated, although the dilatational production is not completely negligible near the locations of the maximum mean shear. In addition, from Figure 21 it is obvious that the role of the dilatational production term for the APG case is to augment the total production. For the

shear production, the $-\overline{u_1'u_2'}\frac{\partial \overline{U_2}}{\partial x_1}$ term is approximately zero across wake, due to the fact that $\frac{\partial \overline{U_2}}{\partial x_1} \approx 0$. Thus for the APG case investigated, the shear production is dominated by the first part, i.e., $-\overline{u_1'u_2'}\left(\frac{\partial \overline{U_1}}{\partial x_2}+\frac{\partial \overline{U_2}}{\partial x_1}\right) \approx -\overline{u_1'u_2'}\frac{\partial \overline{U_1}}{\partial x_2}$.

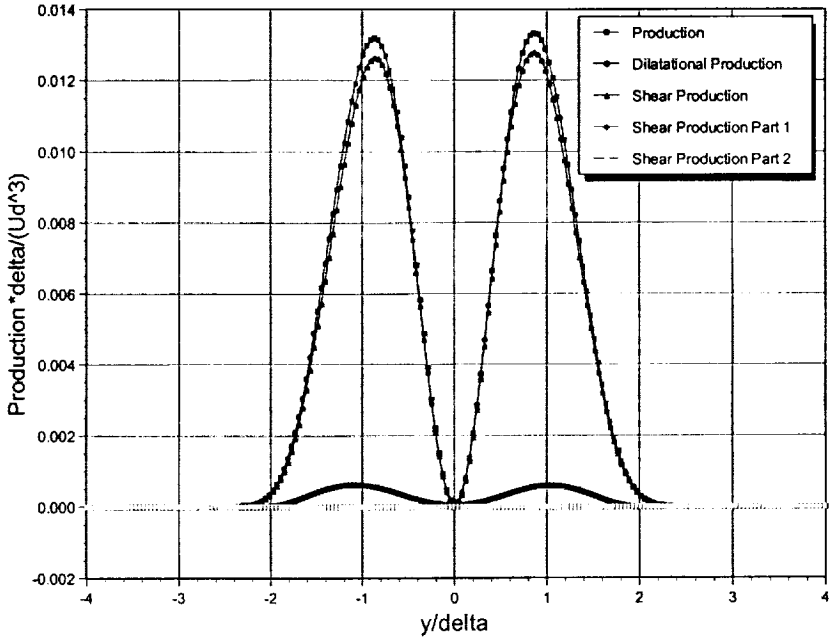

Figure 21. Production Term of Symmetric Wake at APG at x/θ_0 =141.

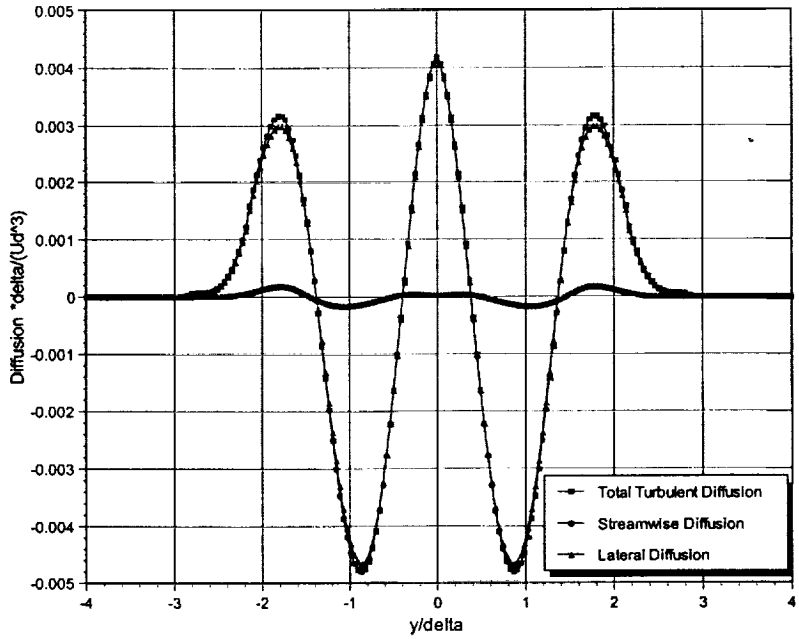

Figure 22. Turbulent Diffusion Term of Symmetric Wake at APG at x/θ_0 =141.

4.3.3 Turbulent Diffusion Term

Figure 22 shows the profile of the turbulent diffusion for the symmetric wake in APG as obtained at $x/\theta_0 = 141$. It can be seen from this figure that like the ZPG case, the lateral turbulent diffusion $-\frac{\partial}{\partial x_2}\overline{\frac{1}{2}(u_1'^2u_2' + u_2'^3 + u_2'u_3'^2)}$ is the dominant turbulent diffusion mechanism and the streamwise turbulent diffusion $-\frac{\partial}{\partial x_1}\overline{\frac{1}{2}(u_1'^3 + u_1'u_2'^2 + u_1'u_3'^2)}$ is negligible. To verify the accuracy of the measurement of the diffusion term, the profile of the total turbulent diffusion term was integrated across wake. The integration is essentially zero.

4.3.4 Dissipation Term

As described in Section 4.2.4, the estimate of the dissipation term for the APG case was conducted via four different approaches: (a), the isotropic turbulence assumption approach, (b), the locally axisymmetric turbulence assumption approach, (c), the semi-isotropic assumption approach and (d) the forced TKE balance approach. Comparison of the dissipation estimate results with these four different approaches presented in Figure 23.

As in the ZPG case, there are significant disparities among the dissipation estimates based on the four approaches for the symmetric wake at APG. Again the isotropy assumption underestimates the dissipation term, while the semi-isotropy assumption over-estimates the dissipation. Once again, the dissipation estimate based on the locally axisymmetric assumption leads to an approximately zero lateral integration of the pressure diffusion term, suggesting that the locally axisymmetric assumption approach is most appropriate for the dissipation estimate for the wake flow in APG.

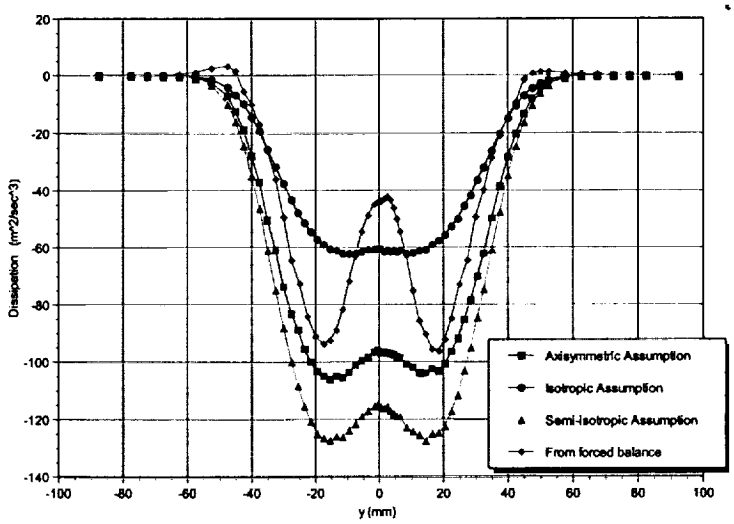

Figure 23. Comparison of dissipation estimate with different approaches for APG at $x/\theta_0 = 141$.

4.3.5 Turbulent Kinetic Energy Budget

The turbulent kinetic energy budget for the symmetric wake in adverse pressure gradient at $x/\theta_0 = 141$ is presented in Figure 24. Error bars associated with the measured terms based on uncertainty analysis are also shown in this figure. Again, as in the ZPG case, the pressure diffusion profile shown in Figure 24 is obtained by forcing a balance of the TKE equation. Actually, this so-called pressure diffusion profile consists of both the true pressure diffusion and the total error of the whole measurement.

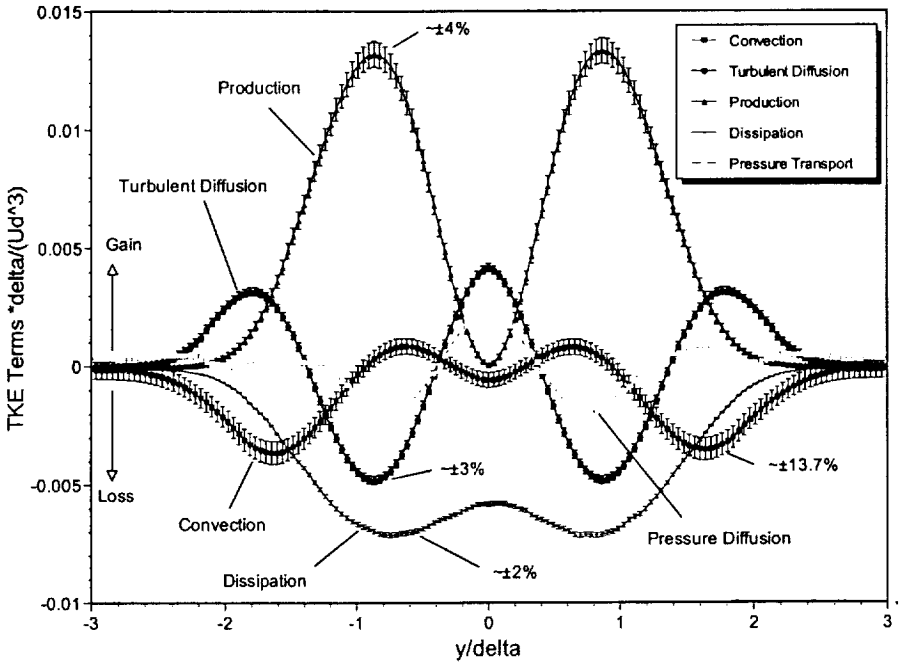

Figure 24. Turbulent Kinetic Energy Budget of Symmetric Wake at APG at $x/\theta_0 = 141$.

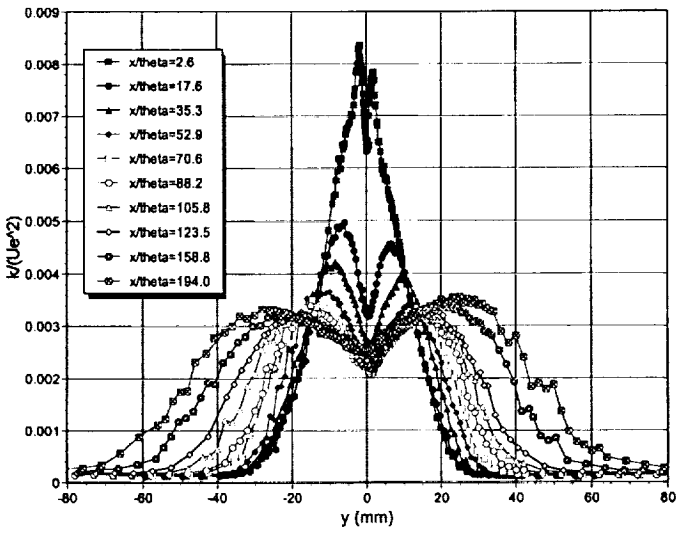

Figure 25. Streamwise Development of Turbulent Kinetic Energy of Symmetric Wake at APG

The interpretation of TKE budget of APG case shown in Figure 24 is similar to that for the ZPG case shown in Figure 16. However, there is one difference between the APG and ZPG turbulence kinetic energy budget that needs to be highlighted. For the APG case, near the center of the wake, the dissipation is not so intense as in the ZPG case. After the aggregation of the gain and loss due to production, diffusion and the dissipation near the center of the wake, there is still a surplus of the turbulence kinetic energy that is convected to the downstream stations. Correspondingly, we should observe an increase of turbulence kinetic energy in the adjacent downstream stations. This is supported by Figure 25 which shows the streamwise development of the turbulence kinetic energy for the APG case.

4.4 Turbulent Kinetic Energy Budget in Favorable Pressure Gradient

4.4.1 Convection Term

Figure 26 shows the convection term for the symmetric wake in favorable pressure gradient as obtained at x/θ_0 =141. Again, near the center of the wake, the streamwise convection $-\overline{U_1}\frac{\partial}{\partial x_1}\left(\frac{\overline{q^2}}{2}\right)$ dominates. Like the APG case shown in Figure 19, the lateral convection $-\overline{U_2}\frac{\partial}{\partial x_2}\left(\frac{\overline{q^2}}{2}\right)$ is quite significant in magnitude near the edge of the wake for the FPG case. But this time, the lateral convection at the edge of the wake results in a local loss of the turbulence kinetic energy since the inward V-component carries turbulence kinetic energy away to downstream stations. As a result, the total loss of the turbulence kinetic energy of the local system is augmented. This convection mechanism near the edge of the wake is different from that of the APG case, in which the streamwise convection contributes a loss while the lateral convection contributes a gain to the local TKE balance system.

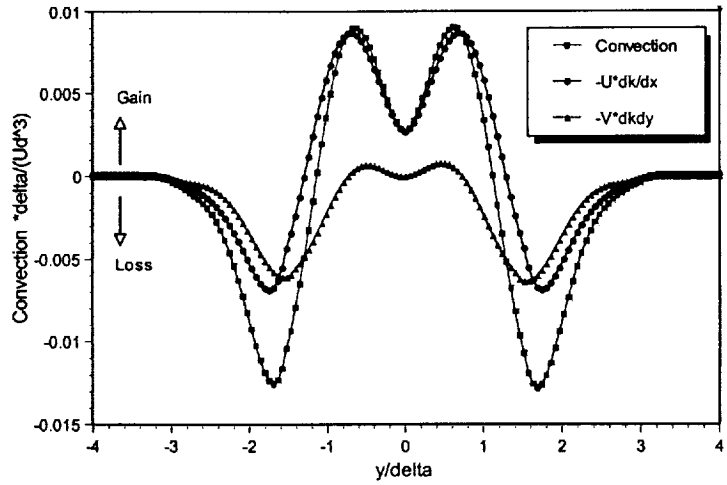

Figure 26. Convection Term of Symmetric Wake at FPG at x/θ_0 =141.

4.4.2 Production Term

Figure 27 shows the turbulence production of the symmetric wake in FPG at $x/\theta_0 = 141$. The designations in this figure are the same as used previously in Section 4.3.2. Again like the ZPG and APG cases, the wake flow in FPG case is shear dominated, although the dilatational production is not completely negligible near the locations of maximum mean shear. Unlike the APG case in which the dilatational production term augments the total production, for the FPG case, the dilatational production is actually a counter-production term and its effect is to reduce the total production. Again like the APG case, the $-\overline{u_1'u_2'}\frac{\partial \overline{U_2}}{\partial x_1}$ term is approximately zero across wake, due to the fact that $\frac{\partial \overline{U_2}}{\partial x_1} \approx 0$. Thus for the FPG case investigated, the shear production is dominated by the first part, i.e., $-\overline{u_1'u_2'}\left(\frac{\partial \overline{U_1}}{\partial x_2}+\frac{\partial \overline{U_2}}{\partial x_1}\right) \approx -\overline{u_1'u_2'}\frac{\partial \overline{U_1}}{\partial x_2}$.

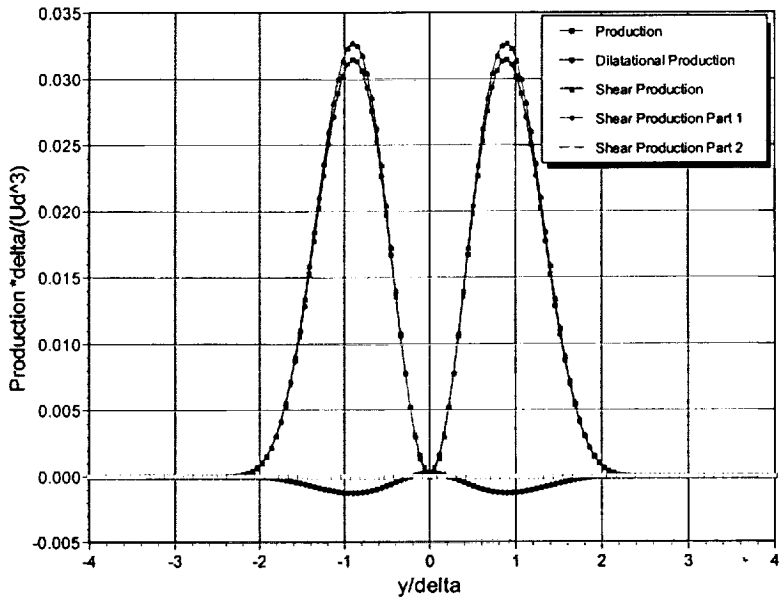

Figure 27. Production Term of Symmetric Wake at FPG at x/θ_0 =141.

4.4.3 Turbulent Diffusion Term

Figure 28 shows the profile of the turbulent diffusion for the symmetric wake in FPG at $x/\theta_0 = 141$. Similar to the ZPG and the APG cases, the lateral turbulent diffusion $-\frac{\partial}{\partial x_2}\overline{\frac{1}{2}\left(u_1'^2u_2'+u_2'^3+u_2'u_3'^2\right)}$ is the dominant turbulent diffusion mechanism and the streamwise turbulent diffusion $-\frac{\partial}{\partial x_1}\overline{\frac{1}{2}\left(u_1'^3+u_1'u_2'^2+u_1'u_3'^2\right)}$ is negligible for the FPG case. To verify the accuracy of the measurement of the diffusion term, the profile of the total turbulent

diffusion term is integrated across wake. The integration result is essentially zero as one would expect.

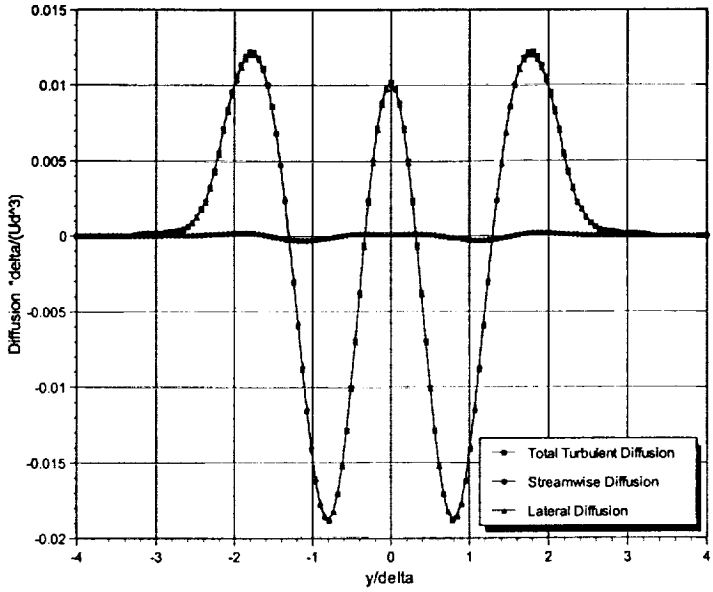

Figure 28. Turbulent Diffusion Term of Symmetric Wake at FPG at x/θ_0 =141.

4.4.4 Dissipation Term

As described in ZPG and APG cases, the estimate of the dissipation term for the FPG case was again conducted via four different approaches: (a), the isotropic turbulence assumption approach, (b), the locally axisymmetric turbulence assumption approach, (c), the semi-isotropic assumption approach and (d) the forced TKE balance approach. Comparison of the dissipation estimate results with these four different approaches presented in Figure 29.

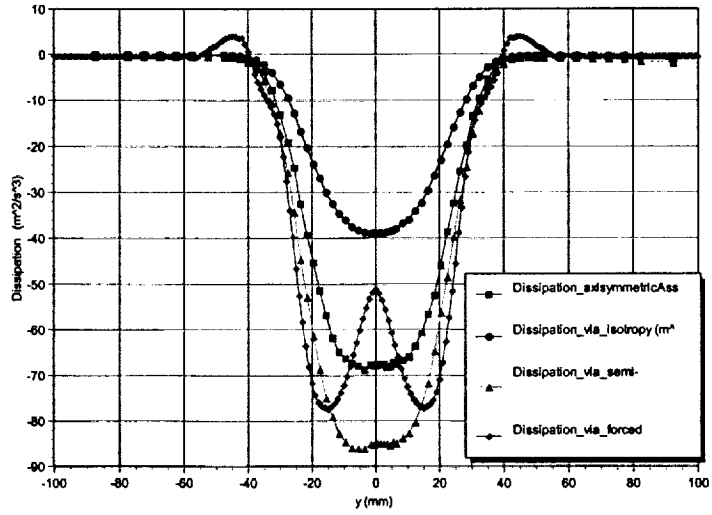

Figure 29. Comparison of dissipation estimate with different approaches for FPG at x/θ_0 =141.

As in the ZPG and APG cases, the isotropy assumption underestimates the dissipation term, while the semi-isotropy assumption over-estimates the dissipation. Once again, the dissipation estimate based on the locally axisymmetric assumption leads to an approximately zero lateral integration of the pressure diffusion term, suggesting that the locally axisymmetric assumption approach is also most appropriate for the dissipation estimate for the wake flow in FPG.

4.4.5 Turbulent Kinetic Energy Budget

The turbulent kinetic energy budget for the symmetric wake in favorable pressure gradient at $x/\theta_0 = 141$ is presented in Figure 30. Again, as in the ZPG and APG cases, the pressure diffusion profile shown in Figure 30 is obtained by forcing a balance of the TKE equation.

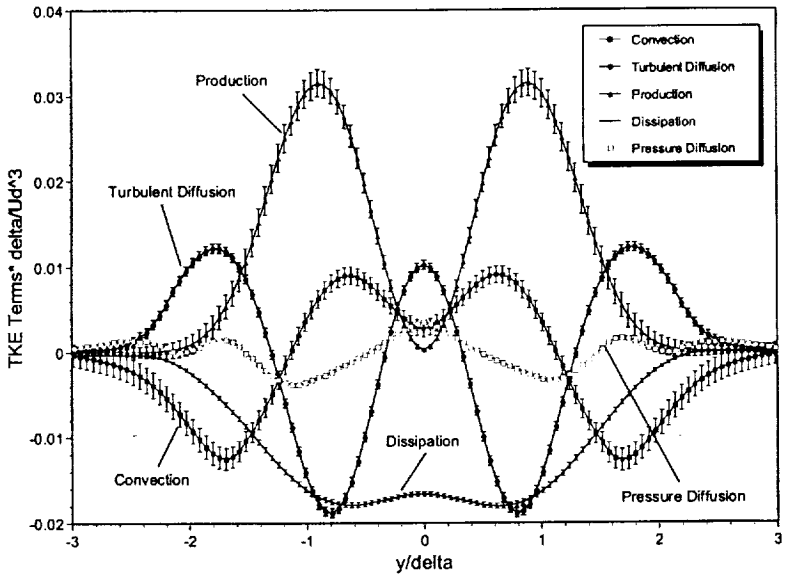

Figure 30. Turbulent Kinetic Energy Budget of Symmetric Wake at FPG at $x/\theta_0 = 141$.

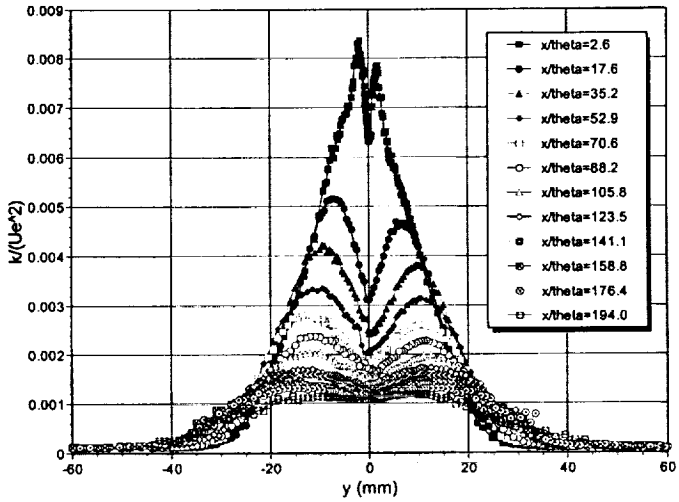

Figure 31. Streamwise Development of Turbulent Kinetic Energy of Symmetric Wake at FPG

The interpretation of TKE budget for the FPG case shown in Figure 30 is similar to that for the ZPG and APG cases. Unlike the APG case, through the central region of the wake, there is a considerable gain of turbulence kinetic energy due to convection. This is consistent with Figure 31, that shows the streamwise development of the turbulence kinetic energy for the FPG case.

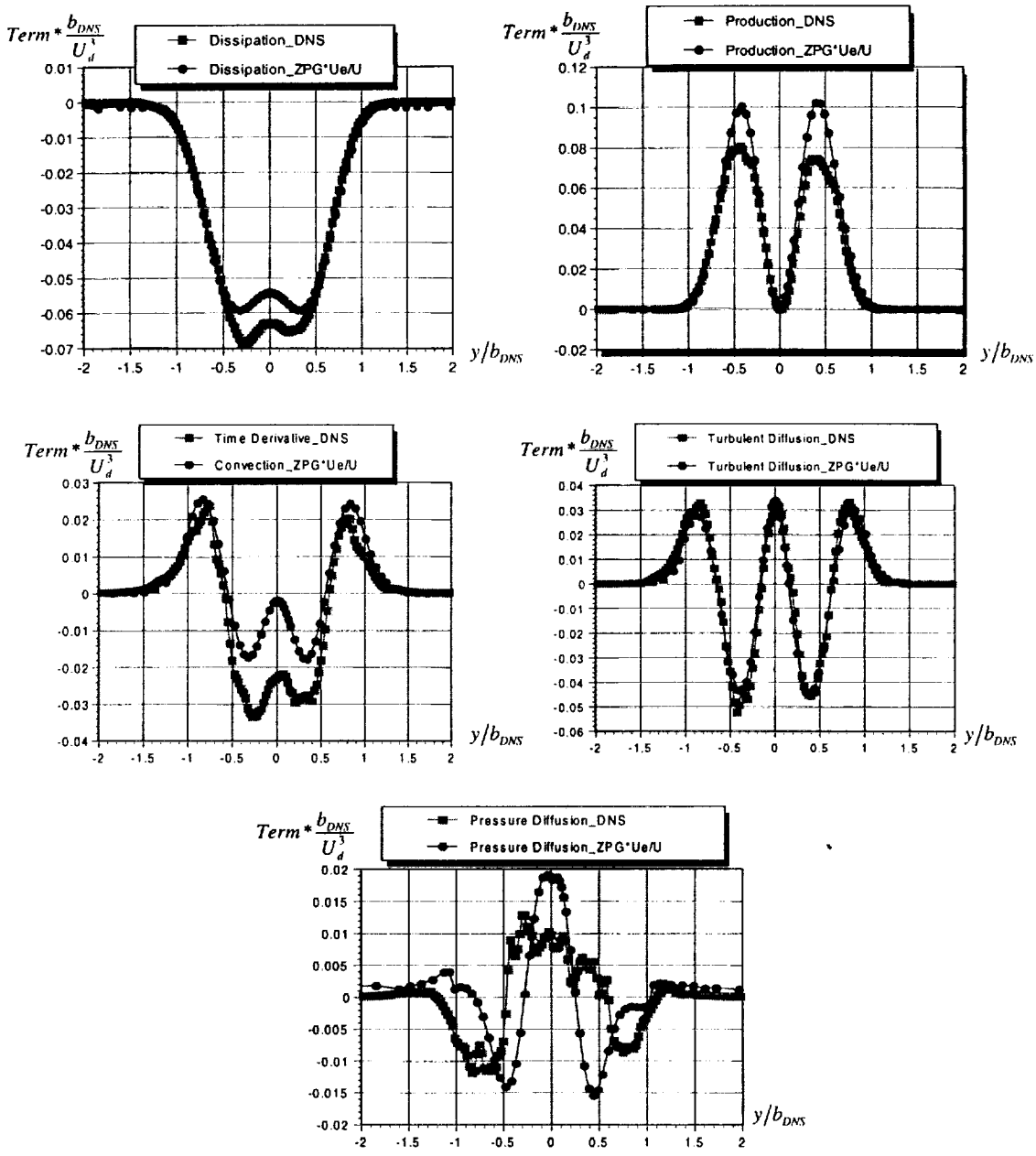

Figure 32. Comparison of TKE Budget Profiles of Symmetric Wake at ZPG with DNS(Moser, Rogers & Ewing, 1998) Result.

4.5 Comparison of the Turbulent Kinetic Energy Budget at ZPG with the DNS Result

Moser, Rogers and Ewing[24] (1998) studied the turbulence kinetic energy budget of a temporally evolving plane wake based on direct numerical simulation (DNS) results. To facilitate their DNS simulation, they picked a section of spatially developed wake and let the wake develop in the temporal domain and then compute the turbulence quantities in the similarity region of the temporal-involving wake. They applied "forcing" to the initial wake and then investigated the influence of the "forcing" on the development of the wake. Their "unforced" wake corresponds to the ZPG conditions of our wake research, with two basic differences: (1) they obtained the TKE budget in the similarity region while ours is obtained in the near wake region and (2) their wake develops in the temporal domain while ours develops in the spatial domain. The spatially and temporally evolving wakes can be made equivalent by utilizing the initial wake velocity defect Ud as the convective velocity as specified by the DNS simulation, with the condition that the lateral convection term can be neglected for the ZPG case. Based on these assumptions, we were able to make direct comparison of the experimental TKE budget profiles with the DNS TKE budget profiles.

Figure 32 shows the comparison of the convection, production, turbulent diffusion, dissipation and the pressure diffusion profiles between the experimental and the DNS results. Considering that the wake develops at different stages and at different Reynolds numbers for the experiment and the DNS simulation, one must admit that the agreement between the experimental and the DNS results is quite encouraging. In particular, the agreement on the turbulent diffusion term is quite good. The experimental and the DNS turbulent diffusion profiles almost overlap each other. Even the comparison of the pressure diffusion term between the experimental and the DNS simulation shows a qualitative agreement. It must be remembered that the experimental pressure diffusion term contains not only the pressure diffusion itself, but also the total measurement error of the TKE budget. Thus the comparison of the pressure diffusion term can be regarded as a measure indicating the accuracy and reliability of the TKE budget measurement. The disparities between the convection, production and dissipation terms can be attributed to the Reynolds number and the different stages of development between the experimental and the DNS data. Moreover, the disparity between the convection term of the experimental and DNS data may also be attributed to the neglect of the lateral convection for the DNS simulation, which evolves in time as a parallel flow. Also it should be pointed out that the scatter of the DNS data points for the pressure diffusion term may be due to an insufficient period for the time averaging of the pressure diffusion term in DNS simulation.

4.6 Effect of the Pressure Gradient on Planar Wake TKE Budget

To investigate the influence of the pressure gradient on the wake TKE budget, the TKE budget terms for the ZPG, APG and FPG cases were normalized by using the local wake half-width, δ, and the square root of the local maximum kinetic energy, $k_{max}^{\frac{1}{2}}$, as the

reference length and velocity scales, respectively. The comparisons of the normalized TKE budget terms for different pressure gradient cases are presented in Figure 33.

Figure 33(d) shows that the scaled dissipation profile does not change very much when the wake is subjected to different pressure gradients. The effect of the imposed pressure gradient is most significant on the convection term, as shown in Figure 33(a). since this term is directly related to the mean motion of the flow field. Correspondingly, as an adjustment of the disparities due to the influence of the pressure gradient on the convection term, the turbulent diffusion and production terms will also change accordingly at different imposed pressure gradient, as shown in Figure 33 (b) and (c). These comparisons indicate that the fundamental TKE transport mechanism is not altered by the imposed pressure gradient. It seems that the imposed pressure gradient exerts its influence on the turbulence field through the mean flow and largest motions rather than the small turbulence in the wake flow.

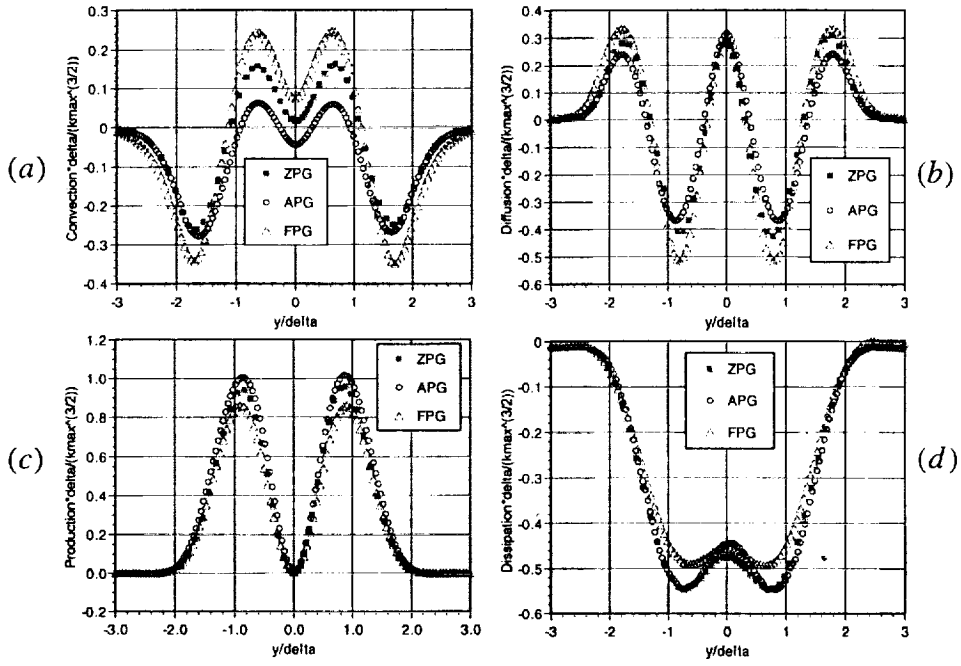

Figure 33. Comparison of TKE Budget Profiles of Symmetric Wake at ZPG, APG and FPG.

5. CONCLUSIONS

Conclusions resulting from the Year-Three wake research can be outlined as follows:

- The TKE budget measurement has been conducted for the symmetric wake in constant zero, adverse and favorable pressure gradients in the near wake region at a Reynolds number of 2.4×10^6 (based on the chord length of splitter plate and a free stream velocity of 30.0 m/s).

- The experimental procedure was carefully designed on the basis of the uncertainty analysis to ensure the reliability of the experimental data. The maximum error associated with TKE budget measurement is less than 15% to the 95% confidence level.
- Four different approaches, based on the isotropic turbulence assumption, the locally axisymmetric homogeneous turbulence assumption, the semi-isotropic turbulence assumption and the forced balance of the TKE budget equation, were applied for the estimate of the dissipation term. The approach based on locally axisymmetric homogeneous turbulence assumption gives the most accurate estimate of the dissipation term for all three pressure gradient cases.
- Comparison of the TKE budget in ZPG case with DNS (Moser, Rogers & Ewing 1998) results indicates good agreement and suggests that the TKE budget measurement procedure and results are reliable for the APG and FPG cases as well.
- Comparison of the appropriately normalized TKE budget terms for APG, ZPG and FPG cases shows that the imposed pressure gradient does not change the fundamental flow physics process for the turbulent kinetic energy transport. It seems that the imposed pressure gradient exerts its influence through the mean flow and large scale structures with the small scale adjusting accordingly.

In a follow-on grant, we will conduct the flow field survey for the wake flow subjected to pressure gradients comparable to these encountered in actual high-lift applications. A tandem airfoil configuration will be used for the pressure field generation.

6. REFERENCES

[1]Liu, X., Thomas, F.O. and Nelson, R.C., 1999, An Experimental Investigation of Wake Development in Arbitrary Pressure Gradients, AIAA paper 99-0677.

[2]Thomas, F.O., Liu, X. and Nelson, R.C., 1997, Experimental Investigation of the Confluent Boundary Layer of a High-Lift System, AIAA paper 97-1934.

[3]Thomas, F.O., Nelson, R.C. and Liu, X., 2000, Experimental Investigation of the Confluent Boundary Layer of a High-Lift System, AIAA Journal, Vol. 38, No. 6, pp978-988.

[4]Brooks, G., Numerical Simulation of a Planar Turbulent Wake in Arbitrary Pressure Gradient, M.S. Thesis, University of Notre Dame, 1999.

[5]Liu, X; Thomas, F.O. and Nelson, R.C., 1998, Asymmetric Wake Development and Structure in Arbitrary Pressure Gradients, Bulletin of the American Physical Society, Vol. 43, No. 9, p2006.

[6]Liu, X., Thomas, F.O., and Nelson, R.C., 1999, Experimental and Numerical Investigation of Pressure Gradient Effects on Asymmetric Wake Development, Bulletin of the American Physical Society, Vol. 44, No. 8, pp133-134.

[7]Duquesne, N., Carlson, J.R., Rumsey, C.L. and Gatski, T.B., Computation of Turbulent Wake Flows in Variable Pressure Gradient, AIAA paper 99-3781, 1999.

[8]Wygnanski, I. and Fiedler, H., 1969, Some Measurements in the Self-preserving Jet, *J. Fluid. Mech.*, vol. 38, part 3, pp. 577-612.

[9]Gutmark, E and Wygnanski, , 1976, The Planar turbulent Jet, *J. Fluid. Mech.*, vol. 73, part 3, pp. 465-495.

[10]Panchapakesan, N.R. and Lumley, J.L., 1993, Turbulence Measurements in Axisymmetric Jets of Air and Helium. Part 1. Air Jet. *J. Fluid. Mech.*, vol. 246, pp. 197-223.

[11]Hussein, H.J., Capp, S.P. and George, W.K., 1994, Velocity Measurements in a High-Reynolds-number, Momentum-conserving, Axisymmetric, Turbulent Jet, *J. Fluid. Mech.*, vol. 258, pp. 31-75.

[12]Heskestad, G., 1965, Hot-Wire Measurements in a Plane Turbulent Jet, *Transactions of ASME, Journal of Applied Mechanics*, December, 1965, pp. 721-734.

[13]Raffoul, C.N., Nejad, A.S. and Gould, R.D., 1995, Investigation of Three-dimensional Turbulent Transport behind a Bluff Body, *FED-vol.217, Separated and Complex Flows, ASME*, pp. 121-128.

[14]Browne, L.W., Antonia, R.A. and Shah, D.A., 1987, Turbulent Energy Dissipation in a Wake, *J. Fluid. Mech.*, vol. 179, pp. 307-326.

[15]Patel, V.C. and Sarda, O.P., 1990, Mean-flow and Turbulence Measurements in the Boundary Layer and Wake of a Ship Double Model, *Experiments in Fluids*, vol. 8, pp. 319-335.

[16]Faure, T. and Robert G., 1996, Turbulent Kinetic Energy Balance in the Wake of a Self-propelled Body, *Experiments in Fluids*, Vol. 21, pp268-274, 1996

[17]Wygnanski, I. and Fiedler, H.E., 1970, The Two-dimensional Mixing Region, *J. Fluid. Mech.*, vol. 41, part2, pp. 327-361.

[18]Zhou, M.D., Heine, C. and Wygnanski, I., 1996, The effects of excitation on the coherent and random motion in a plane wall jet, *J. Fluid. Mech.*, vol. 310, pp. 1-37.

[19]George, W.K. and Hussein, H.J., 1991, Locally Axisymmetric Turbulence, *J. Fluid. Mech.*, vol. 233, pp. 1-23.

[20]Hinze, J.O., Turbulence, McGraw-Hill Book Company, 1975.

[21]Meyers, J.F., 1985, The Elusive Third Component, FED Vol.33, International Symposium on Laser Anemometry, the Winter Annual Meeting of the ASME, Miami Beach, Florida, November 17-22, 1985.

[22]Wallace, J.M. and Foss, J.F., 1995, The Measurement of Vorticity in Turbulent Flows, *Annual Review of Fluid Mechanics*, vol. 27, pp. 469-514.

[23]Demuren, A.O., Rogers, M.M., Durbin, P. and Lele, S.K., 1996, On Modeling Pressure Diffusion in Non-homogeneous Shear Flows, Proceedings of the Summer Program 1996, Center of Turbulent Research, Stanford University.

[24]Moser, R.D., Rogers, M.M., and Ewing, D.W., 1998, Self-similarity of Time-evolving Plane Wakes, *J. Fluid. Mech.*, vol. 367, pp. 255-289.

APPENDIX A

Determination of the Optimal Spacing between Measurement Stations

A1 Lagrangian Interpolation and Central Difference Scheme

The streamwise derivatives in the TKE budget were estimated from the data taken at three consecutive streamwise measurement stations. A natural approach for taking the spatial derivative of function f(x) based on might be first taking the Lagrangian interpolation, denoted by p(x), as expressed in Equation (A1), through the three arbitrary spatially separated nodal points and then taking the derivative of the Lagrangian interpolation, as shown in Figure A1.

$$f(x) \approx p(x) = \frac{(x-x_i)(x-x_{i+1})}{(x_{i-1}-x_i)(x_{i-1}-x_{i+1})} y_{i-1} + \frac{(x-x_{i-1})(x-x_{i+1})}{(x_i-x_{i-1})(x_i-x_{i+1})} y_i + \frac{(x-x_{i-1})(x-x_i)}{(x_{i+1}-x_{i-1})(x_{i+1}-x_i)} y_{i+1} \tag{A1}$$

However, for $x_i = x$, $x_i - x_{i-1} = h$ and $x_{i+1} - x_i = h$, we have

$$\frac{df}{dx} \approx \frac{dp}{dx} = \frac{y_{i+1} - y_{i-1}}{2h} \tag{A2}$$

which is the central difference scheme. This demonstrates that the numerical differentiation based on the even-spaced quadratic Lagrangian polynomial interpolation is identical to the central difference scheme. In other words, the central difference scheme is based on the implicit assumption that the curve passing through the three nodal points is a quadratic Lagrangian polynomial. From Gerald and Wheatly (1994), the error term of the derivative based on Lagragian interpolation is

$$\frac{df}{dx} - \frac{dp}{dx} = \prod_{\substack{j=0 \\ j \neq i}}^{n} (x_i - x_j) \frac{f^{(n+1)}(\xi)}{(n+1)!} \Bigg|_{\substack{n=2 \\ x_i = x \\ x_i - x_{i-1} = h \\ x_{i+1} - x_i = h}} = -\frac{h^2}{3!} f'''(\xi) \tag{A3}$$

which is again identical to the truncation error term of the central difference scheme. Thus, the true value of $\frac{df}{dx}$ can be expressed as

$$\frac{df}{dx} = \frac{dp}{dx} + error = \frac{y_{i+1} - y_{i-1}}{2h} - \frac{h^2}{3!} f'''(\xi) \tag{A4}$$

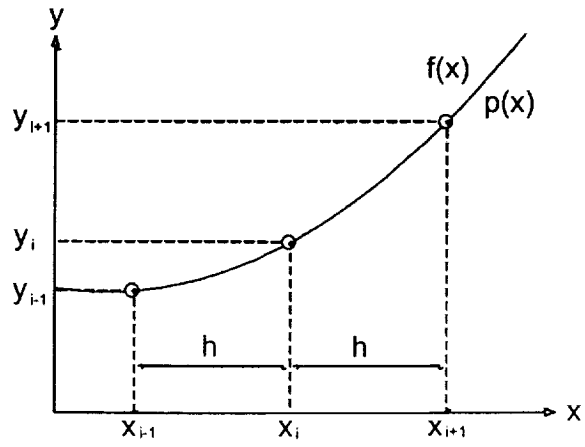

Figure A1. Lagrangian Interpolation.

A2 Uncertainty of the Streamwise Derivative

Let $D = \frac{y_{i+1} - y_{i-1}}{2h}$, $\delta_t = -\frac{h^2}{3!} f'''(\xi)$, then

$$\frac{df}{dx} = D + \delta_t . \tag{A5}$$

Ideally, if there is no positioning error associated with the movement of the measuring probes, the error of the estimate of $\frac{df}{dx}$ is solely determined by δ_t, which is in nature a bias error due to the use of the central difference scheme. This error will increase if h increases. So ideally, we want the spacing between the two measurement stations as close as possible. However, in reality, there are positioning errors associated with the streamwise and lateral locations, i.e., x and y laboratory positions of the probe. With the consideration of this positioning error, the behavior of the total uncertainty of $\frac{df}{dx}$ will be totally different. Let δh and δy be the positioning errors associated with x and y coordinates, respectively. Then the propagation of these errors to the quantity δD can be estimated as

$$\delta D = \sqrt{\left(\frac{\partial D}{\partial h}\delta h\right)^2 + \left(\frac{\partial D}{\partial y_{i+1}}\delta y_{i+1}\right)^2 + \left(\frac{\partial D}{\partial y_{i-1}}\delta y_{i-1}\right)^2} = \sqrt{\frac{(y_{i+1} - y_{i-1})^2}{4h^4}(\delta h)^2 + \frac{1}{2h^2}(\delta y)^2} \tag{A6}$$

The uncertainty of δ_t due to the positioning error is

$$\delta(\delta_t) = \sqrt{\left(\frac{\partial \delta_t}{\partial h}\right)^2 (\delta h)^2} = \frac{h\,\delta h}{3} f'''(\xi) \tag{A7}$$

Finally, the total uncertainty of the streamwise derivative $\frac{df}{dx}$ is given by

$$\delta\left(\frac{df}{dx}\right) = \sqrt{(\delta D)^2 + (\delta(\delta_t))^2 + (\delta_r)^2} = \sqrt{\underbrace{\frac{(y_{i+1} - y_{i-1})^2}{4h^4}(\delta h)^2 + \frac{1}{2h^2}(\delta y)^2 + \left(\frac{h}{3} f'''(\xi)\right)^2 (\delta h)^2}_{\text{Random Error}} + \underbrace{\left(\frac{h^2}{3!} f'''(\xi)\right)^2}_{\text{Bias Error}}} \tag{A8}$$

A3 The Optimal Spacing between Measurement Stations

As indicated in Equation (A8), the final total uncertainty of $\frac{df}{dx}$ comprises two parts, the random error part and the bias error part. The variations of these two parts with h are different, as shown in Figure A2 and A3 in which the comparisons of the total uncertainty of dk/dx and dU/dx and the corresponding random and bias error parts are shown. Obviously, the first two terms in the random error part dominate the random error behavior, decreasing as h increases. However, the bias error increases as h increases. The two competing parts give rise to the optimal separation h. Based on these two plots, one can choose roughly the optimal separation of the measurement station as roughly around 5 in.

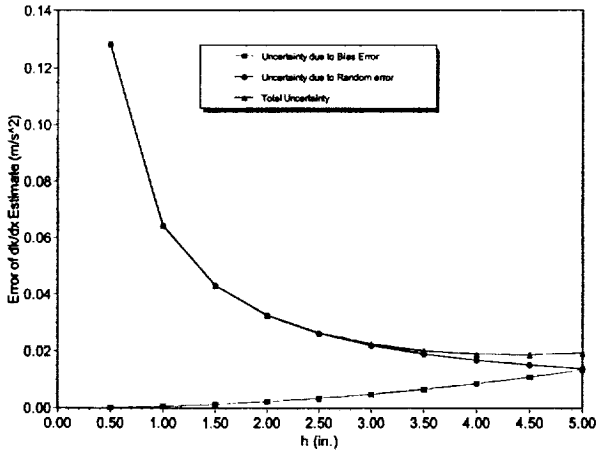

Figure A2. Uncertainty Analysis of dk/dx for ZPG at x=40in, y/δ =0.

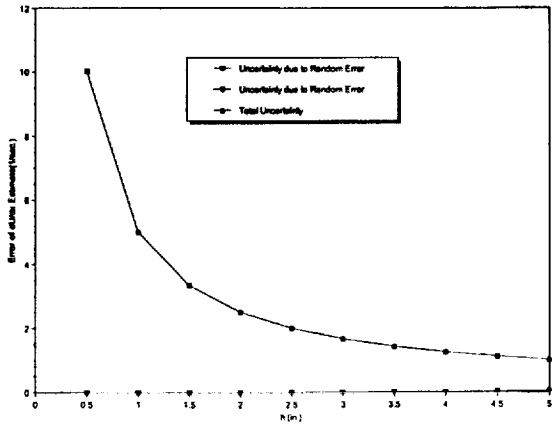

Figure A3. Uncertainty Analysis of dU/dx for ZPG at x=40in, y/δ=0

A4 Location of Measurement Stations

The above analysis shows the optimal spacing between the streamwise measurement stations is roughly 5 in.. For our TKE budget measurement, we choose x=35, 40 and 45in as the locations for the streamwise measurement stations and the TKE budget is estimated at x=40in location for ZPG, APG and FPG cases. This region of measurement is located roughly in the middle of the imposed pressure gradient zone in the diffuser test section and any possible ambiguity due to the end effect of the diffuser test section can be avoided with this arrangement of the measurement stations.